Running Title: Role of FERONIA in Root Hair Tip-Growth

Functional Characterization of *fer-ts,* a Temperature-Sensitive FERONIA Mutant Allele That Alters Root Hair Growth

Daewon Kim[1, 3], Fangwei Gu[3], Sung Jin Park[3], Jonathon Combs[3], Alexander Adams[2], Heather B. Mayes[2], Jeong Dong Bahk[1] and Erik Nielsen[3]

[1]*Division of Applied Life Sciences (BK21plus), Graduate School of Gyeongsang National University, Jinju 660-701, Republic of Korea*

[2]*Department of Chemical Engineering, University of Michigan, Ann Arbor, MI 48109, USA.*

[3]*Department of Molecular, Cellular, and Developmental Biology, University of Michigan, Ann Arbor, Michigan 48109*

Corresponding author: E. Nielsen; e-mail: nielsene@umich.edu

E.N. conceived the original screening and research plans; J-D.B. and E.N. supervised the experiments; D.K., F.G., S-J.P., and J.C. performed the in planta experiments and microscopy, and A.A. performed structural modeling and was supervised by H.B.M. D.K. wrote the article with contributions of all the authors; E.N. supervised and completed the writing, and agrees to serve as the author responsible for contact and ensures communication.

ABSTRACT

In plants, root hairs undergo a highly-polarized form of cell expansion called tip-growth, in which cell expansion is restricted to the root hair apex. In order to characterize cellular components playing a role in this specialized form of cellular expansion we screened for conditional temperature sensitive (ts) mutants by EMS mutagenesis. Here we describe one of these mutants, *fer-ts* (*fer*onia-*t*emperature *s*ensitive). Mutant *fer-ts* seedlings grew normally at permissive temperatures (20˚C), but failed to form root hairs at non-permissive temperatures (30˚C). Map based-cloning and whole genome sequencing revealed that *fer-ts* resulted from a G41S substitution in the extracellular domain of *FERONIA* (*FER*). A functional fluorescent fusion of FER containing the *fer-ts* mutation maintained a plasma membrane localization at both permissive and non-permissive temperatures, but that the *fer-ts* allele was subject to enhanced protein turnover at elevated temperatures. Mutant *fer-ts* seedlings were resistant to added RALF1 peptide at non-permissive temperatures, supporting a role for *FER* in perception of this peptide hormone. Additionally, at non-permissive temperatures *fer-ts* seedlings displayed altered ROS accumulation upon auxin treatment and phenocopied constitutive *fer* mutant responses to a variety of plant hormone treatments. Molecular modeling and sequence comparison with other CrRLK1L receptor family members revealed that the mutated glycine in *fer-ts* is highly conserved, but significantly removed from recently characterized RALF23 and LORELI-LIKE-GLYCOPROTEIN (LLG2) binding domains, perhaps suggesting that *fer-ts* phenotypes may not be directly due to loss of binding to RALF1 peptides.

Key words: FERONIA, root hair, tip growth, CrRLK1L receptor kinase, RALF.

INTRODUCTION

In higher plants, root hairs are cellular protuberances resulting from the polarized outgrowth of specialized root epidermal cells, known as trichoblasts (Gilroy and Jones, 2000). Development of root hair can be divided into three phases: cell specification, initiation of bulge formation, and polarized tip growth (Cho and Cosgrove, 2002).

Polarized tip growth is precisely modulated due to the highly localized exocytosis of Golgi-derived vesicles and the deposition of cell wall material at a restricted area of the root hair tip region, and a tip-concentrated cytoplasmic calcium ion (Ca^{2+}) gradient ensures correct targeting of this polarized membrane trafficking (Hepler et al., 2001; Smith et al., 2005; Cole and Fowler, 2006). This calcium ion gradient is established by localized generation of reactive oxygen species (ROS) by *ROOT HAIR DEFECTIVE2* (*RHD2*) which encodes an NADPH oxidase in *A. thaliana* (Foreman et al., 2003). RHO OF PLANTS (ROP) small GTPases mediated signal transduction is involved in specifying the root hair initiation site, and future root hair elongation by stimulating *RHD2* activity at the growing root hairs tip apex (Molendijk et al., 2001; Jones et al., 2002; Carol and Dolan, 2006). Recently, a number of receptor-like kinases (RLKs) have been identified that are involved in cellular growth regulatory mechanisms, especially in cell elongation associated with root hair tip growth in higher plants (Shiu and Bleecker, 2001; Lehti-Shiu et al., 2009; Lindner et al., 2012).

The plant RLK family has more than 600 members in *Arabidopsis*, divided into 44 subfamilies depending on their N-terminal domains (Shiu and Bleecker, 2001; Greeff et al., 2012). While RLKs have been implicated in many biologically important processes, a number of subfamilies within this superfamily have been implicated in

monitoring of cell wall integrity and cell wall properties (Feng et al., 1995). In particular, CrRLK1L subfamily proteins, which includes *FER* (Huck et al., 2003), *EREBUS* (*ERE*) (Haruta et al., 2014), *THESEUS1* (*THE1*) (Hematy et al., 2007), *ANXUR1/2* (Miyazaki et al., 2009), have been implicated in cell wall sensing associated with a variety of cellular events such as female fertility, cell elongation, root-hair development, mechanosensing, and responses to hormones and pathogens (Boisson-Dernier et al., 2009; Cheung and Wu, 2011; Lindner et al., 2012).

The CrRLK1L subfamily is named after the first member functionally characterized in *Catharanthus roseus* cell cultures (Schulze-Muth et al., 1996), and Arabidopsis, contains 17 CrRLK1L subfamily members (Hematy and Hofte, 2008). The majority of CrRLK1L receptor-like kinase proteins are predicted serine/threonine kinases with a single transmembrane between an N-terminal extracellular domain and a C-terminal cytoplasmic kinase domain (Cheung and Wu, 2011). The CrRLK1L proteins have an extracellular domain with two domains showing limited homology to the carbohydrate-binding domain of animal malectin proteins (Schallus et al., 2008).

In the CrRLK1L subfamily, *THE1* was discovered in a screen for suppressors that partially restored the dark-grown hypocotyl growth defect of *procuste1-1(prc1-1)*, which is defective in the cellulose synthase catalytic subunit CESA6 (Hematy et al., 2007). *THE1* is localized to the plasma membrane (PM) of elongating cells and in vascular tissues. *THE1* loss- and gain-of-function plants do not appear to display significant growth defects in wild-type backgrounds, but these mutants altered the growth and ectopic lignification in a number of plants with defects in cell wall integrity (Hematy et al., 2007). Another member of CrRLK1L subfamily, *HERCULES1* (*HERK1*), was identified as functionally redundant with *THE1* in modulating cell

elongation (Guo et al., 2009). While mutant *herk1* plants displayed normal growth, *the1 herk1* double mutants were severely stunted (Guo et al., 2009). In addition, HERK1 has an autophosphorylation activity and is highly phosphorylated in the kinase domain *in planta* (Guo et al., 2009). In addition, *ANXUR1* and *ANXUR2* (*ANX1* and *ANX2*), are exclusively expressed in the male gametophyte (Boisson-Dernier et al., 2009). *ANX1* and *ANX2* are responsible for maintaining pollen tube wall integrity during migration through floral tissues, and their deactivation is thought to allow the pollen to burst during fertilization (Boisson-Dernier et al., 2009). These proteins are localized to growing pollen tube tips, and appeared to be associated with vesicles involved in polarized membrane trafficking during tip growth (Boisson-Dernier et al., 2009).

Similar to *ANX1* and *ANX2*, and *FER*, which is allelic to *SIRÈNE (SRN),* was initially identified in the regulation of female control of fertility (Huck et al., 2003). Interestingly, *FER* is highly expressed in the synergid cells of the female gametophyte and in a variety of vegetative tissues, but not in the male gametophyte (Escobar-Restrepo et al., 2007; Guo et al., 2009). In the female gametophyte, *FER* is involved in sensing pollen tube arrival and promoting its rupture, (Huck et al., 2003; Rotman et al., 2003), in the initiation of programmed cell death of one of two synergid cells during this double fertilization event (Ngo et al., 2014), and in the inhibition of polyspermy through regulation of demethylesterified pectin accumulation in the filiform apparatus of the ovule (Duan et al., 2020). In addition to important roles during fertilization, *FER* has also been shown to regulate aspects of root hair elongation (Duan et al., 2010; Huang et al., 2013), calcium signaling during mechanical stimulation of roots (Shih et al., 2014), and cell wall responses to both abiotic and biotic stress (Huck et al., 2003; Rotman et al., 2003; Lindner et al., 2012; Duan et al., 2014; Ngo et al., 2014; Shih et al.,

2014; Li et al., 2016). *FER* was identified as a ROP guanidine exchange factor 1 (ROPGEF1) interacting partner by yeast two-hybrid screening for root hair tip-growth in Arabidopsis (Duan et al., 2010). More recently, *FER*, and other members of the CrRLK1L receptor families have been proposed to bind to secreted RALF (rapid alkalinization factor) peptide ligands (Haruta et al., 2014), with RALF1, binding the *FER* extracellular domain to suppress cell elongation of the primary root (Haruta et al., 2014), and RALF23 binding *FER* during plant immune responses (Xiao et al., 2019).

Although several mutants of *FER* have been previously described, we have identified a new temperature-sensitive mutation (*fer-ts*) in a highly conserved glycine residue (G41S) present in the extracellular domain of the FER receptor kinase, as well as other members of the CrRLK1L receptor-like kinase family and mammalian malectin sequences. The *fer-ts* mutant exhibited rapid and dramatically decreased root hair tip-growth upon transferal from permissive temperature to non-permissive growth temperature. Additionally, *fer-ts* mutants were partially insensitive to RALF1 peptide induced root elongation inhibition at non-permissive temperatures, showed altered root growth characteristics compared to wild-type plants when exposed to auxin, and displayed reduces ROS accumulation. Cessation of root hair tip growth occurred within five minutes of transfer to non-permissive temperatures, and observation that a fluorescently-tagged version of the temperature-sensitive FER(G41S)-EYFP mutant was still correctly targeted to the plasma membrane at these early time points, suggests that the primary defect of this mutant is due to failure to properly transmit extracellular signals at non-permissive temperatures.

155

156

RESULTS

Isolation of a temperature-sensitive mutant that inhibits root hair tip growth

The regulatory GTPase, RabA4b, participates in membrane trafficking associated with the polarized secretion of cell wall components in plant cells. In addition, loss of tip localization of EYFP-RabA4b is highly correlated with inhibition of root hair tip growth (Preuss et al., 2004). In order to understand molecular mechanisms that control root hair tip growth, EMS-mutagenized seeds of a stable transgenic Arabidopsis line expressing EYFP-RabA4b were screened for seedlings with wild-type root hairs at permissive temperatures (20˚C), but which displayed impaired root hair growth when grown at non-permissive temperatures (30˚C). The progeny of approximately 6,000 EMS-mutagenized seeds were screened. From the screening, four temperature-sensitive (ts-) root hair growth defect mutants were isolated, which we initially termed Loss-of-Tip-Localization mutants (*ltl1* to *ltl4*). Among these *ltl ts* mutants, *ltl2*, (subsequently referred to as *fer-ts*) root hair growth characteristics were examined under permissive and non-permissive temperature conditions. In permissive growth conditions (20˚C), *fer-ts* root hairs displayed normal growth, however, both root hair growth and apical accumulation of EYFP-RabA4b of *fer-ts* root hairs were dramatically inhibited at 30˚C (Figure 1a and 1d).

To quantify root hair elongation in *fer-ts* under permissive and non-permissive temperature conditions, both root hair lengths and root hair density were measured. No significant differences were found between wild-type and *fer-ts* either in mature root hair length, or in the number of root hairs per unit root length when plants were grown at 20˚C. However, both length of root hairs and root hair density were greatly reduced in *fer-ts* in plants grown at 30˚C (Figure 1c and 1d). Primary root length and root

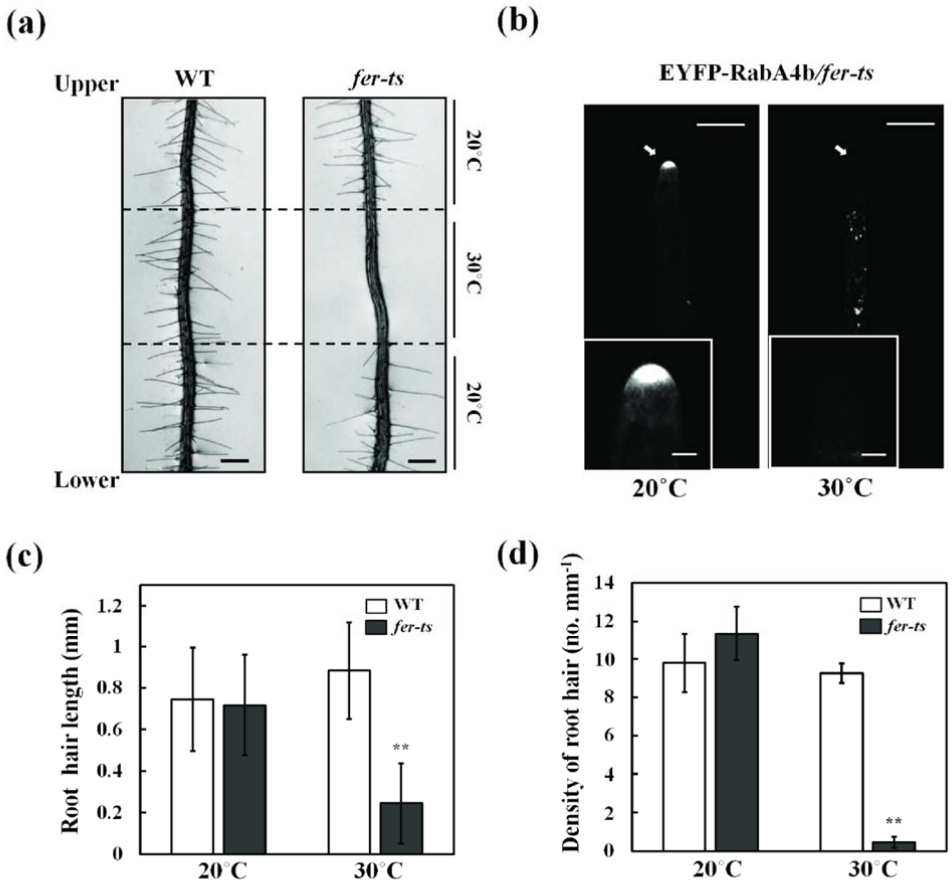

Figure 1. Isolation of a temperature-sensitive root hair growth defect mutant.
(a) Seven day-old seedling plants were grown vertically in 1/4 MS media under 20˚C and transferred to 30˚C for 6 h, followed by 24 h recovery at 20ºC. Bright field images were collected with a Nikon Eclipse E600 wide-field microscope with a 20x Plan Apo DIC (n.a. 0.75) lens. Dashed lines indicate root tip positions when seedling plants were transferred to 30˚C condition for 6 hours, and again when they were transferred back to 20˚C. Scale bars = 200 µm. (b) Localization of EYFP-RabA4b protein in growing root-hair cells of *fer-ts* mutant at 20˚C and 30˚C. Medial root hair sections were collected using spinning-disk confocal microscopy from growing root-hair cells of seven-day-old seedlings stably expressing EYFP-RabA4b in the *fer-ts* mutant in 20ºC (left) or 30ºC (right) using a Zeiss 40x Plan-Apochromat (n.a. 1.3) lens and appropriate EYFP fluorescence filter sets. Scale bars = 10 µm. Insets, magnified images to show details of EYFP-RabA4b subcellular localization in root-hair tips. Scale bars = 2 µm. (c) Quantification of root hair length in WT and *fer-ts* mutants under 20˚C (wild-type (n=392), fer-ts (n=454)) and 30˚C (wild-type (n=185), fer-ts (n=23)) conditions. (d) Calculation of root hair densities in WT and *fer-ts* mutants at 20˚C (wild-type (n=392), fer-ts (n=454)) and 30˚C (wild-type (n=185), *fer-ts* (n=23)) in fully expanded primary roots of seven-day old plants. In each case, root hair lengths and densities were measured from n=20 individual seedlings. Error bars represent SD. **p<0.001 by Student's t-test.

growth rates of *fer-ts* seedlings were only slightly reduced compared with those of wild-type at 30˚C (See Supplemental Figure S1). These results indicated that, at least in early stages of seedling growth and development *fer-ts* temperature sensitive defects are largely specific to root hair elongation in non-permissive temperature conditions.

In order to characterize effects of the *fer-ts* mutation on root hair growth

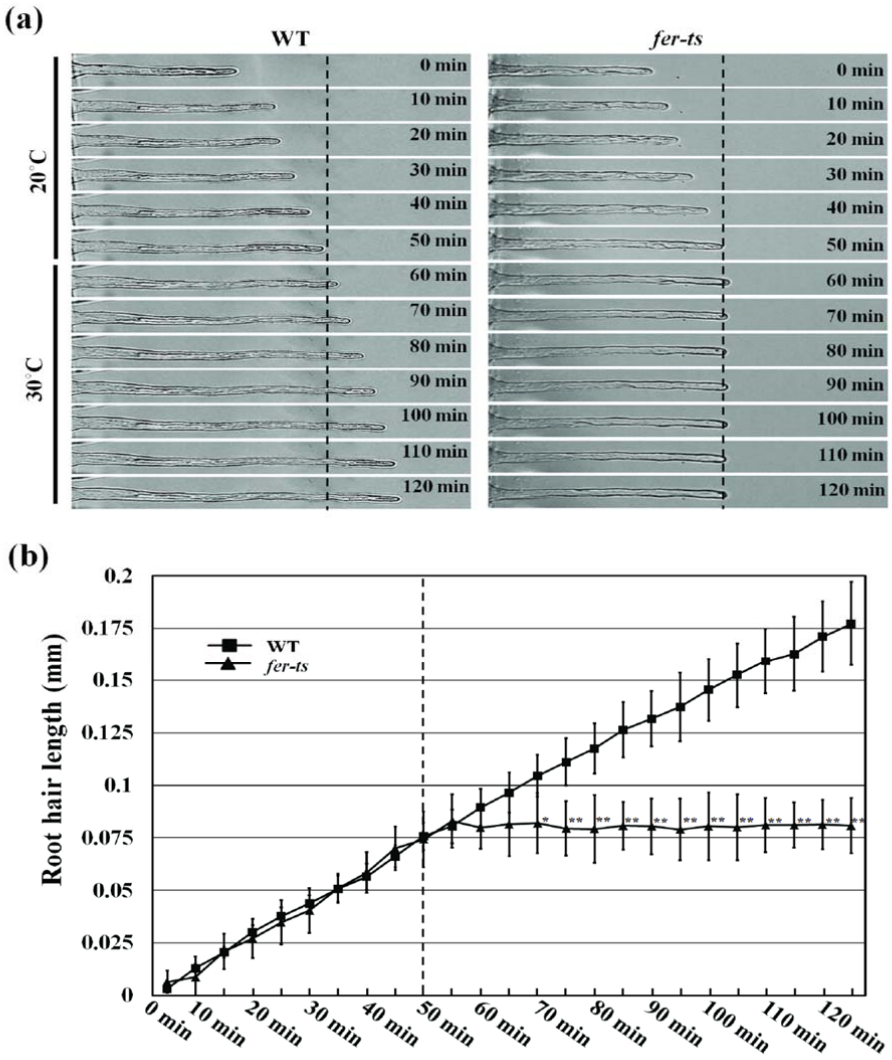

Figure 2. Root hair growth dynamics in WT and *fer-ts* seedlings.
(a) Root hair tip-growth in WT and *fer-ts* mutant plants under permissive (20ºC) and non-permissive (30ºC) temperatures by time-lapse microscopy. Bright field images of growing root hairs of WT and *fer-ts* mutant plants were collected every minute by time-lapse microscopy using a Zeiss 40x Plan-Apochromat (1.3 NA) lens. Representative images of WT and *fer-ts* mutant root hair elongation are presented at 10 min intervals. (b) Quantitative analysis of WT (n=4) and *fer-ts* mutant (n=4) root hair lengths upon transition to 30˚C. WT (black squares) and *fer-ts* (black triangles) mutant root hair elongation were measured every five minutes and root hair lengths were determined using the measure function in Image J (1.44 version) The dashed line indicates transition from 20ºC to 30ºC. Error bars represent SD. *p<0.05, **p<0.01 by Student's t-test.

dynamics, elongating root hairs were visualized by time-lapse microscopy for two hours. Seven day-old *fer-ts* seedlings were placed in a temperature-controlled plant growth chamber at 20˚C for 50 min and then the temperature of the chamber was rapidly transitioned to 30˚C (Figure 2). While root hair growth was unaffected by temperature

transition in wild-type plants, transition from permissive to non-permissive temperatures resulted in rapid cessation of tip-growth in the *fer-ts* mutant (Figure 2 and Movie S1). The rapid kinetics of inhibition of *fer-ts* root hair growth within 5-10 minutes would be consistent with rapid inactivation of *fer-ts* protein function at the plasma membrane.

The polarized cell expansion that occurs in root hairs is driven by specific targeting of newly-synthesized cell wall cargo to the growing apex of the root hair cell (Nielsen, 2008; Cheung and Wu, 2011). Delivery of this cell wall cargo, which occurs by polarized membrane trafficking, is associated with the tip-localized accumulation of membrane compartments labeled by the small regulatory GTPase, RabA4b (Preuss et al., 2004). EYFP-RabA4b was detected in the apical region of growing *fer-ts* root hairs at 20˚C, but tip localization of EYFP-RabA4b was rapidly lost upon transition to 30˚C (Figure 3). Because the apical accumulation of EYFP-RabA4b compartments has been tightly linked to polarized expansion in root hair cells (Preuss et al., 2004; Preuss et al., 2006; Thole et al., 2008), we examined how these compartments were affected by the transition from permissive to non-permissive growth temperatures (Figure 3a). EYFP-RabA4b accumulation was examined in *fer-ts* plants in a temperature-controlled chamber at 20˚C for 14 min, and then the chamber was rapidly transitioned to 30˚C (Figure 3b). Images of growing root hairs were collected at one minute intervals by time-lapse confocal microscopy, and tip-localized EYFP signal was quantified. While tip-localized EYFP-RabA4b signal was unaffected by transition from 20˚C to 30˚C in wild-type root hairs (See supplemental Figure S2), tip-localized EYFP-RabA4b was significantly reduced within one minute of the transition from 20˚C to 30˚C (Figure 3b and 3c). Significantly, this reduction coincided with both elevated chamber temperature

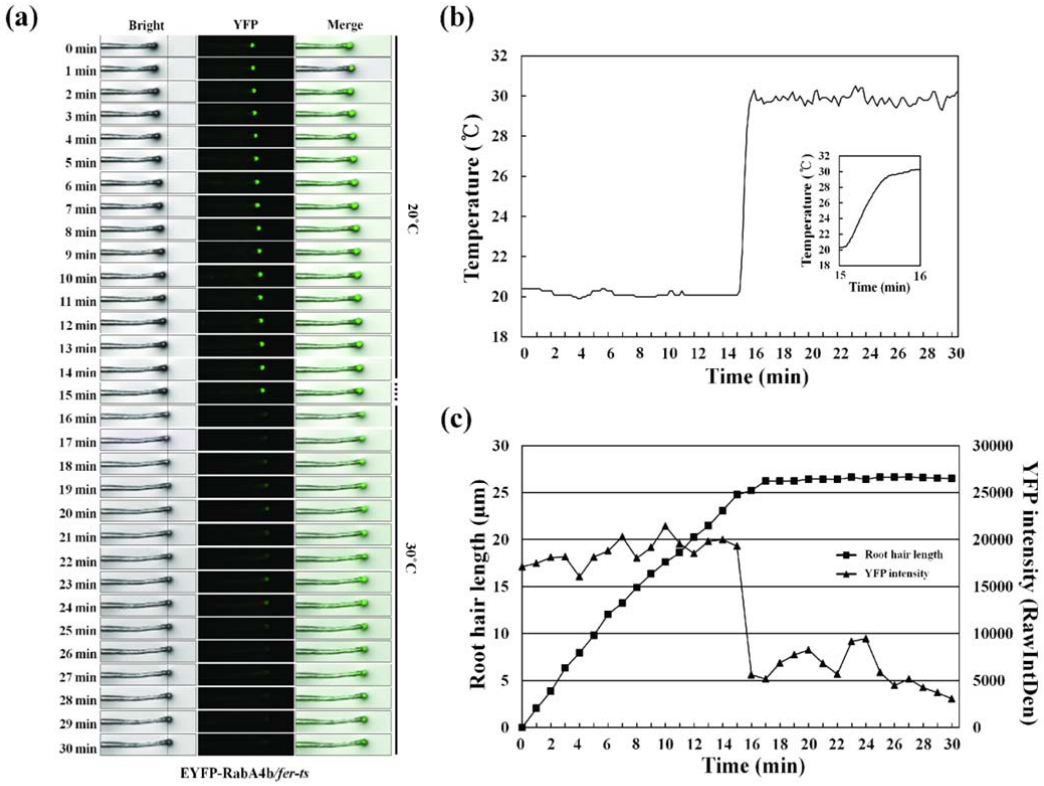

Figure 3. Temperature-sensitive subcellular dynamics of EYFP-RabA4b labeled compartments in growing root hairs in *fer-ts* mutants.

(a) Localization of EYFP-RabA4b protein in growing root-hair cells of *fer-ts* mutant at permissive (20ºC) or non-permissive (30ºC) temperature conditions. Growing *fer-ts* root hairs were imaged at one minute intervals for 30 min at 20˚C at which the growth chamber temperature was raised to 30˚C. For each time point, both bright field (Bright) and fluorescence (YFP) images were collected sequentially, and tip-localized EYFP-RabA4b compartments were monitored by spinning-disk fluorescence confocal microscopy using a Zeiss 40x Plan-Apochromat (1.3 NA) lens with appropriate EYFP fluorescence filter sets. The dashed line indicates the temperature transition from 20˚C to 30˚C. Merge indicates overlapped images of bright and EYFP fluorescent signals. (b) Monitoring of chamber temperatures of *fer-ts* mutant. Insert, transition of the growth chamber temperature from 20˚C up to 30˚C were measured every 1 min by dry air thermostat situated in close proximity (~2 mm) from the growing root hair. (c) Quantification of root hair elongation and EYFP-RabA4b root hair tip localization. Root hair length and EYFP-RabA4b fluorescence were quantified by Image J (1.44 version) program every 1 min.

and cessation of tip-growth (Figure 3c).

Map-based cloning and full-genome sequencing of the *fer-ts* locus

To identify the mutant locus responsible for the rapid, temperature-sensitive loss of root hair elongation and tip-localized EYFP-RabA4b, map-based cloning and full-genome sequencing was performed. F_2 mapping populations were obtained by reciprocal crosses of back-crossed mutants (Col-0) with L*er* wild-type plants (Bell and Ecker, 1994).

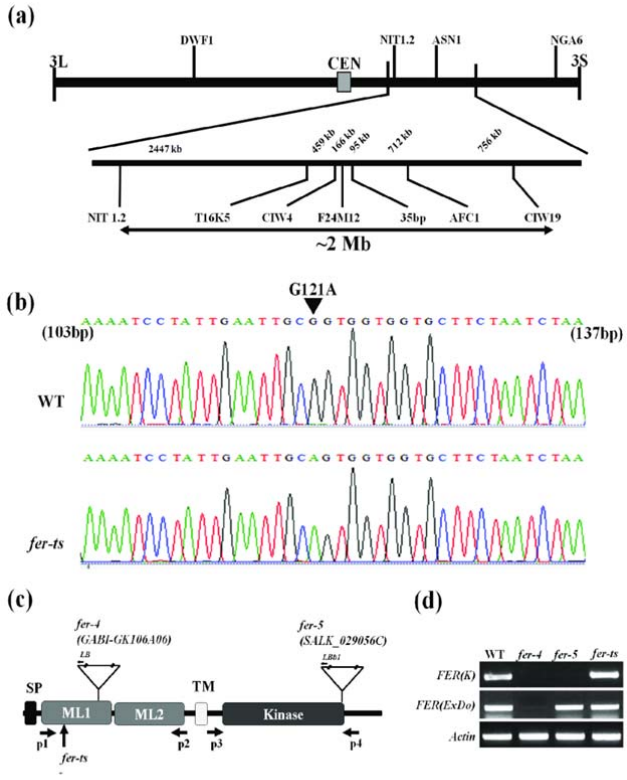

Figure 4. Map-based cloning of *fer-ts*.
(a) A linear diagram of the Arabidopsis third chromosome is shown, with a magnified F24M12 marker region displayed below. The centromere is indicated with filled-rectangle. Low-resolution map-based cloning resulted in identification of the fer-ts locus within an approximately 2 Mb region of chromosome III bounded by markers NIT1.2 and CIW19 (Double headed arrow). (b) SNPs specific to the ts-mutant within this region were identified using whole genomic resequencing, followed by targeted resequencing of genomic DNA sequencing of *fer-ts* and wild-type parental lines. A single G-to-A substitution was found in FERONIA (At3g51550). The arrowhead indicates G121A substituted mutation in the *FERONIA* gene locus. (c) Schematic diagram of FERONIA protein domains and mutation regions, composed of an N-terminal extracellular domain (tandem repeat malectin-like domains; ML1 and ML2), TM (transmembrane) domain in the middle region and a C-terminal kinase domain (serine/threonine kinase), end of N-terminus has signal peptide (SP) sequence for plasma-membrane trafficking. The *fer-4* and *fer-5* mutants displayed that T-DNA was inserted in malectin-like domain 1 and kinase domain, respectively. (d) RT-PCR analysis of T-DNA inserted mutants and EMS mutants. FER (K) and FER (ExDo) was amplified using pair of P1 and P2 primers and P3 and P4 primers, respectively. Actin was used as a loading control.

Segregating F_2 populations were used for the subsequent map-based cloning. The temperature-sensitive mutant lesion was initially located on chromosome 3 between the SSLP markers *NIT1.2* and *NGA6* (Figure 4a). Low-resolution mapping narrowed the location of the mutant locus to an approximately 2 Mb region of chromosome 3. We then performed whole-genome sequencing, and determined that the *fer-ts* mutant locus within this 2 Mb region of chromosome 3 was due to a G121A nucleotide replacement resulting in a G41S substitution mutation within the extracellular domain of the

previously characterized FER receptor-like kinase (Figure 4b and 4c). In order to eliminate the possibility that the G→A substitution that gave rise to the *fer-ts* G41S mutation influenced accumulation of *FER* mRNA at the transcriptional level, we performed RT-PCR analysis. *FERONIA* transcript levels were unchanged from those in wild-type plants (Figure 4d).

fer-ts phenotypes were confirmed by reciprocal crossing with FERONIA mutants and complementation assays

To confirm that the temperature sensitive root hair defects and loss of tip-localized EYFP-RabA4b were causally linked to the G41S mutation in the FER locus, *fer-ts* mutant plants were reciprocally crossed with two previously characterized *FER* mutants, *fer-4* and *fer-5* (Duan et al., 2010). In previous reports, *fer-4* was shown to fully abolish FER protein accumulation, while *fer-5* was shown to accumulate a truncated FER protein missing a functional cytosolic protein kinase domain, although both *fer-4* and *fer-5* mutants displayed constitutive root hair growth defects (Duan et al., 2010). The F1 generation of *fer-ts* crossed to wild-type plants displayed normal root hair growth in both permissive and non-permissive temperature conditions. However, F1 progeny of either *fer-ts* (paternal line) crossed with *fer-4* and *fer-5* mutants (maternal lines; Figure 5a), or *fer-ts* (maternal line) crossed with *fer-4* and *fer-5* mutants (paternal line; Supplemental Figure S3a) displayed ts-phenotypes at non-permissive temperatures, respectively. The F1 generations of reciprocally crossed plants were confirmed by genomic DNA PCR analysis with primers that discriminated between the *fer-ts* (or wild-type) *FER* loci and *fer-4* and *fer-5* T-DNA insertion mutant loci (Figure 5b-c, and Supplemental Figure S3b).

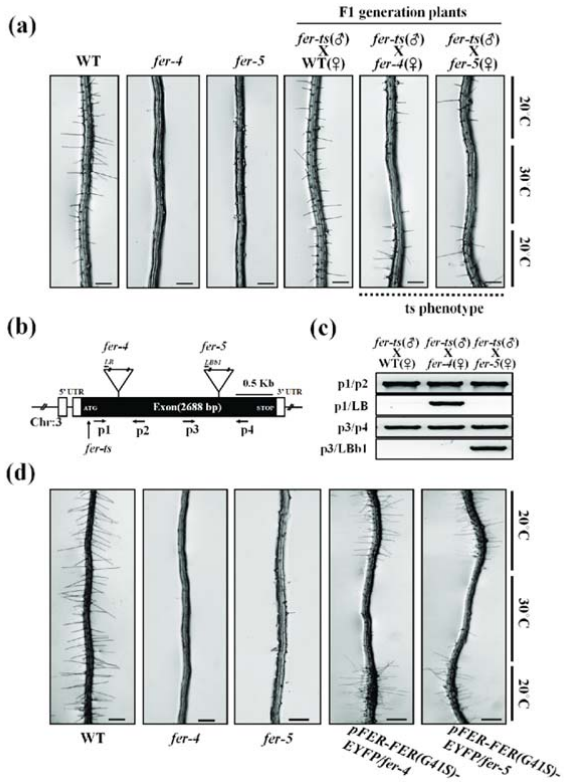

Figure 5. The *fer-ts* mutant confers ts-root hair growth defects when crossed with *fer-4* and *fer-5* mutants.
(a) Wild-type (WT), *fer-4*, *fer-5*, and F1 progeny from crosses (paternal = *fer-ts*, maternal = *fer-4* or *fer-5*) of *fer-ts*/*fer-4* and *fer-ts*/*fer-5* were grown vertically for seven days at 20°C, transferred to 30°C for 6 h, and then grown for an additional 24 h at 20°C. Bright field images were collected with a Nikon Eclipse E600 wide-field microscope with a 20x Plan Apo DIC (0.75 NA) lens. Both *fer-ts*/*fer-4* and *fer-ts*/*fer-5* progeny clearly demonstrated a ts-dependent root hair phenotype. Scale bars = 200 µm. (b) Schematic diagram of the *FERONIA* gene structure. Open and filled boxes indicate untranslated regions (UTRs) and exon regions, respectively. The locations of T-DNA insertion mutants (*fer-4* and *fer-5*) and *fer-ts* are indicated by triangles and arrows, respectively. (c) Genotyping of crossed F1 plants. Genomic DNA was extracted from F1 generation plants and subjected PCR to confirm presence of the *fer-4* and *fer-5* genotypes (d) Both *fer-4* and *fer-5* display temperature-dependent root hair phenotypes when transformed with a fluorescently-tagged FER construct containing the *fer-ts* mutation (pFER-FER(G41S)-EYFP). Seven-day old seedlings were grown vertically for seven days at 20°C, transferred to 30°C for 6 h, and then grown for an additional 24 h at 20°C. Bright field images were collected with a Nikon Eclipse E600 wide-field microscope with a 20x Plan Apo DIC (0.75 NA) lens. Presence of the transgenic pFER-FER(G41S)-EYFP construct clearly demonstrated a ts-dependent root hair phenotype. Scale bars = 200 µm.

To verify that the FER G41S mutation specifically conferred the temperature-sensitive root hair phenotype, a fluorescently tagged FER-EYFP containing the G41S mutation, FER(G41S), driven by endogenous *FER* promoter sequences, was transformed into *fer-4* and *fer-5* mutant plants. Transgenic *fer-4* and *fer-5* plants, expressing mutant FER(G41S)-EYFP proteins rescued root hair growth defects in these two *fer* mutant backgrounds in a temperature-sensitive manner (Figure 5d). Further, a wild-type

fluorescently-tagged FER-EYFP, driven by endogenous FER promoter sequences, was able to fully rescue *fer-ts* root hair defects. FER(WT)-EYFP protein was successfully detected in plasma membranes and pFER-FER(WT)-EYFP in *fer-ts* transgenic lines displayed the normal root hair growth both 20˚C and 30˚C (See Supplemental Figure S4). Taken together, these data strongly support that *fer-ts* phenotype is the result of the G41S mutation of the FERONIA protein.

FERONIA is localized to the plasma membrane and G41S substitution does not alter its subcellular localization at non-permissive temperatures

Previously, GFP-fused FERONIA was shown to localize to plasma membranes in various plant tissues (Duan et al., 2010). In order to confirm the plasma membrane localization of our fluorescently-tagged FER fusions, and examine whether the presence of the G41S mutation affected FER(G41S) subcellular localization, we examined the subcellular distributions of the FER(WT)-EYFP and FER(G41S)-EYFP fusion proteins in stably transformed plants (Figure 6). At permissive temperatures, FER(WT)-EYFP was observed primarily in plasma membranes in various tissues such as leaf, root and root hairs (Figure 6a). Interestingly, FER(WT)-EYFP protein was observed both in plasma membranes and an apical vesicle population in growing root hairs (Movie S2). Magnified images of FER(WT)-EYFP indicated that this fusion protein is almost exclusively plasma membrane localized, and does not display any significant accumulation in intracellular compartments (Figure 6b).

To determine whether the introduction of the G41S substitution in the *fer-ts* mutant might affect its protein stability, we blocked new protein synthesis by treating five-day-old *Arabidopsis* seedlings with cycloheximide, and then compared protein

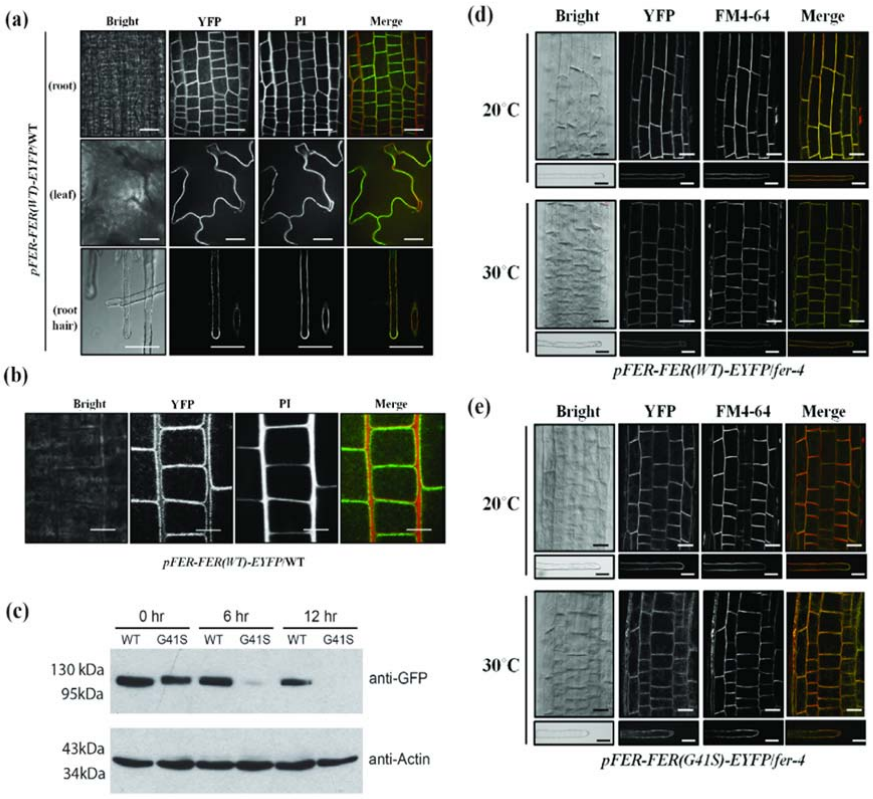

Figure 6. Subcellular localization of FER(WT)-EYFP and FER(G41S)-EYFP fluorescent fusion proteins in stably transformed *Arabidopsis*.

(a) Subcellular localization of FER(WT)-EYFP protein in various tissues. Fluorescent confocal images displaying the subcellular distribution of FER(WT)-EYFP protein was detected from growing root, leaf and root hair cells of seven-day-old seedlings in pFER-FER(WT)-EYFP/WT transgenic plants. Cell walls were counter-stained by incubating for 5 min in a propidium iodide (PI) solution (10 µg/ml). Images were collected by spinning-disk fluorescence confocal microscopy using a Zeiss 40x Plan-Apochromat (1.3 NA) lens with appropriate EYFP and PI fluorescence filter sets. Scale bars = 20 µm. (b) Magnified images of FER(WT)-EYFP fluorescence. FER(WT)-EYFP in wild-type of growing root cells of seven-day-old A. thaliana seedlings was detected by spinning-disc confocal microscopy using a Zeiss 100x Plan-Apochromat (1.46 NA) oil immersion objective with appropriate EYFP and PI filter sets. Scale bars = 10 µm. (c) Protein turnover rates of FER(WT)-EYFP and FER(G41S)-EYFP at non-permissive temperature (30ºC). Five-day old seedling were grown at 20ºC and then treated with 200 µM cycloheximide and transferred to 30ºC. Total proteins were extracted at each time point and the relative levels were determined using immunoblotting with anti-GFP and anti-actin antibodies. FER(G41S)-EYFP levels rapidly decreased during the time course, while levels of FER(WT)-EYFP were not significantly reduced. Actin was used as a loading control. (d-e) Subcellular localization of FER(WT)-EYFP (d) and FER(G41S)-EYFP (e) fluorescent fusions in root and root hair cells at permissive (20ºC) and non-permissive (30ºC) temperatures. Cells were counterstained with FM4-64 to visualize cell walls. Images were collected by spinning-disk fluorescence confocal microscopy using a Zeiss 40x Plan-Apochromat (1.3 NA) lens with appropriate EYFP and FM4-64 fluorescence filter sets. Scale bars = 20 µm; root, 10 µm; root hair.

turnover rates of the FER(WT)-EYFP and FER(G41S)-EYFP proteins when grown at 30°C. Overall accumulation of the FER(G41S)-EYFP was reduced significantly during the time course, but no significant reduction in protein accumulation was not observed for either EYFP(WT)-EYFP or an actin loading control (Figure 6c). These results

suggest that *fer-ts* mutant phenotypes may be associated with enhanced turnover due to protein misfolding.

Since the FER(G41S)-EYFP appeared to be less stable than FER(WT)-EYFP we wanted to check whether might affect the accumulation or subcellular distribution of this protein in plants subjected to non-permissive temperatures. We therefore compared the subcellular distributions of FER(WT)-EYFP and FER(G41S)-EYFP at both 20˚C and 30˚C (Figure 6d and 6e). While no changes in accumulation or distribution of FER(WT)-EYFP were observed in roots and root hairs between 20^{o}C and 30^{o}C conditions (Figure 6c), at 30^{o}C some FER(G41S)-EYFP fluorescence could be observed in internal subcellular membranes, although significant levels of the FER(G41S)-EYFP remained at the plasma membranes in these cells even after incubation at 30˚C for 6 hours (Figure 6e). Furthermore, FER(WT)-EYFP and FER(G41S)-EYFP subcellular distributions were visualized in cells in the root elongation zone every 30 s by confocal microscopy at 20˚C for 10 minutes and then subsequently at 30˚C for an additional 50 minutes. In both FER(WT)-EYFP and FER(G41S)-EYFP seedlings, significant fluorescent signal remained associated with the plasma membranes in the cells in these tissues at both permissive and non-permissive temperatures (Movies S3 and S4). Interestingly, FER(G41S)-EYFP signal detected in internal subcellular membranes was significantly higher when plants were continuously incubated at 30˚C for 24 hours (Supplemental Figure S5). These data, when taken together with the rapid onset (<5 minutes) of mutant root hair growth defects, are consistent with a model in which the mutant FER(G41S) temperature-sensitive phenotypes are caused by inactivation of the receptor-like activities associated with this protein, and are not simply due to destabilization of the protein, or its removal from the plasma membrane.

310

311 **The *fer-ts* displays impaired sensitivity to RALF1 peptides in non-permissive**
312 **temperature conditions**

313 Signaling in the CrRLK1L family of receptor kinases have been linked to a family of
314 small extracellular peptide hormones called rapid alkalinization factors (RALFs;
315 (Haruta et al., 2014; Stegmann et al., 2017). RALF1, which was previously
316 demonstrated to suppress cell elongation of the primary root in Arabidopsis and other
317 plants (Pearce et al., 2001), has now been shown to directly bind with the FER
318 extracellular domain (Haruta et al., 2014; Stegmann et al., 2017). Because the G41S
319 mutation appears to affect protein stability at non-permissive temperatures, perhaps by
320 destabilizing the structure of the extracellular domain of this protein (Figure 6c), we
321 were curious whether RALF1 suppression of primary root elongation would be affected
322 in *fer-ts* mutants. As shown in Figure 7, both wild-type seedlings and *fer-ts* mutants
323 were highly sensitive to active RALF1 peptide under permissive temperature conditions.
324 However, as previously described, the sensitivity of root growth to RALF1 in *fer-5*
325 mutant was reduced in comparison to wild-type plants at 20^{o}C (Figure 7a and 7c).
326 Importantly, sensitivity of *fer-ts* seedlings to RALF1 peptide treatment was dramatically
327 reduced at 30^{o}C, even though wild-type plants and *fer-5* mutants still responded to
328 RALF1 peptide treatment with similar levels of root elongation inhibition (Figure 7b
329 and 7d). These results support the previous determination that RALF1 peptide signaling
330 occurs through the FER receptor-like kinase, and would be consistent with a model in
331 which the G41S mutation results in temperature-sensitive inactivation of the
332 extracellular ligand-binding domain of the FERONIA protein.

333

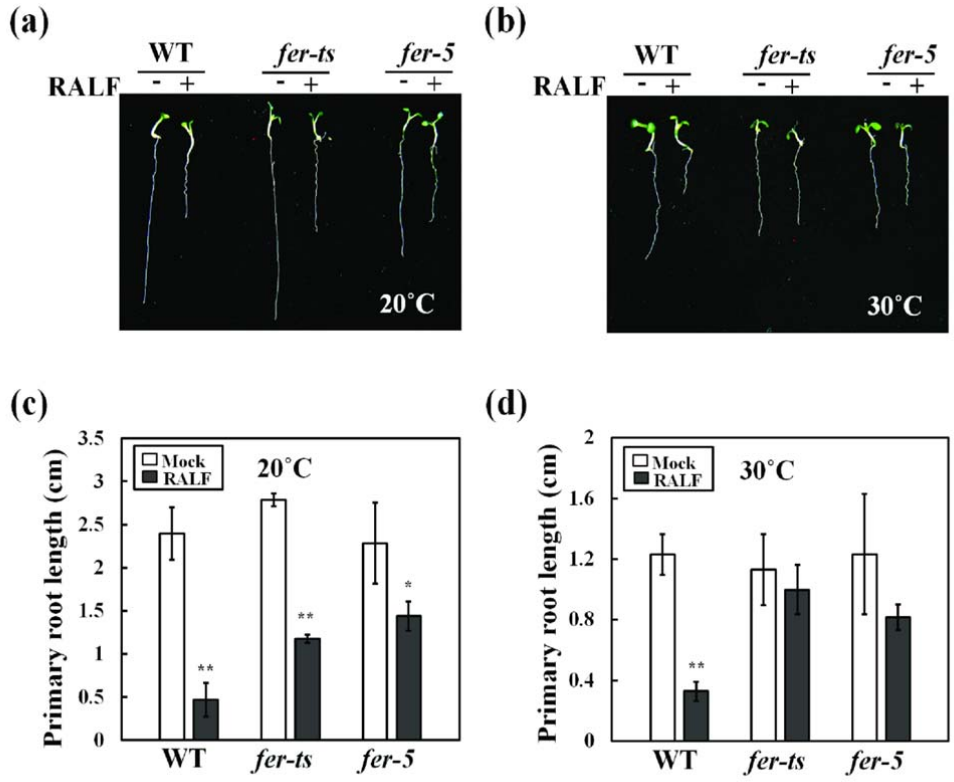

Figure 7. *fer-ts* mutants are partially insensitive to RALF1 peptide mediated root growth inhibition at non-permissive temperatures.

Wild-type (WT), *fer-ts*, or *fer-5* plants were germinated and grown for 3 days in 1/2 MS liquid media at 20°C, and then transferred to 1/2 MS liquid media containing 1uM RALF1 peptide (RALF+) or a mock buffer control (RALF-) and grown an additional 3 days at 20°C (a) or 30°C (b). Images of representative seedlings were collected using an Olympus SZX12 stereoscopic microscope. Quantification of primary root lengths (n = 10 seedlings) in the presence or absence of RALF1 peptide treatment in permissive, 20°C (c) and non-permissive, 30°C (d) conditions. Primary root lengths were determined using Image J. Error bars represent SD. *p<0.05, **p<0.01 by Student's t-test.

ROS accumulation of *fer-ts* was greatly reduced at 30 °C and *fer-ts* phenotype was not rescued by various hormone treatments.

In previous reports, ROS accumulation is highly reduced in *fer-4* and *fer-5* mutants especially in root hair tips and primary roots (Duan et al., 2010). In order to investigate the ROS accumulation, WT and *fer* mutants were treated with H_2DCF-DA to monitor ROS levels. In WT plants, ROS accumulation was observed in primary roots and root hairs, and these levels increased slightly upon NAA treatment at both 20°C and 30°C (Figure 8). While *fer-ts* plants showed similar ROS accumulation patterns as those

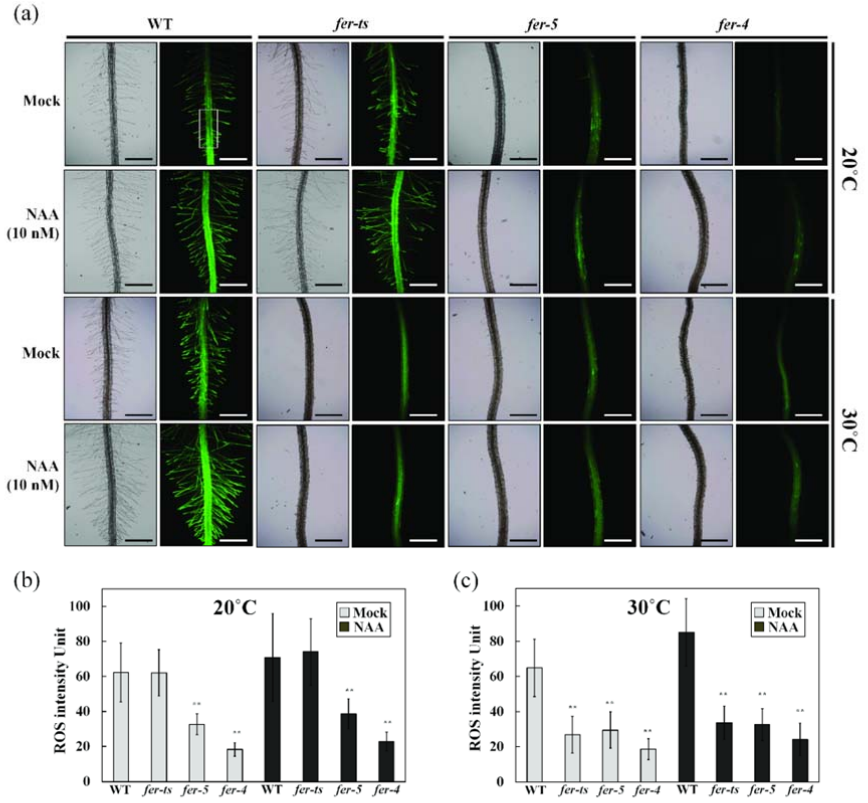

Figure 8. Detection of ROS in WT, *fer-ts* and *fer-5* primary roots and root hairs.
(a) ROS accumulation in permissive and non-permissive temperature conditions with or without auxin treatments. Wild-type (WT), *fer-ts, fer-4,* or *fer-5* seedlings were grown vertically on 1/4 MS media plates for seven days at permissive (20°C) or non-permissive (30 C) temperatures in the presence or absence of (10 nM NAA). Plates were bathed with five ml of 50 uM in H_2DCF-DA suspended in 1/4xMS liquid media for 5 min, followed by two gentle washes with 10 ml of 1/4 MS. Fluorescence images were collected with a Zeiss Axio Imager Z1 fluorescence microscope with 2.5x objective and green (GFP) filter set. The WT ROS image was acquired by auto-exposure, all other images were acquired using the WT exposure conditions. Scale bars = 500 µm. (b) The rectangle in (a) indicates a representative region of interest (ROI) where average ROS intensity was quantified for the samples. Intensities of ROS were quantified by image J program. Error bars represent SD. **p<0.01 by Student's t-test.

observed in wild-type plants at 20°C, at 30°C ROS accumulation was dramatically reduced both in the absence and presence of NAA (Figure 8a). However, while ROS accumulation in the *fer-ts* mutant was strictly temperature dependent (compare Figures 8b and 8c), these reduced ROS levels were similar to those observed at both temperatures for the constitutive *fer-4* and *fer-5* mutants (Figure 8a; compare Figures 8b and 8c)

In order to investigate how broadly the temperature-sensitive *fer-ts* mutant phenocopied *fer-4* and *fer-5* mutants, these three mutants were treated with several

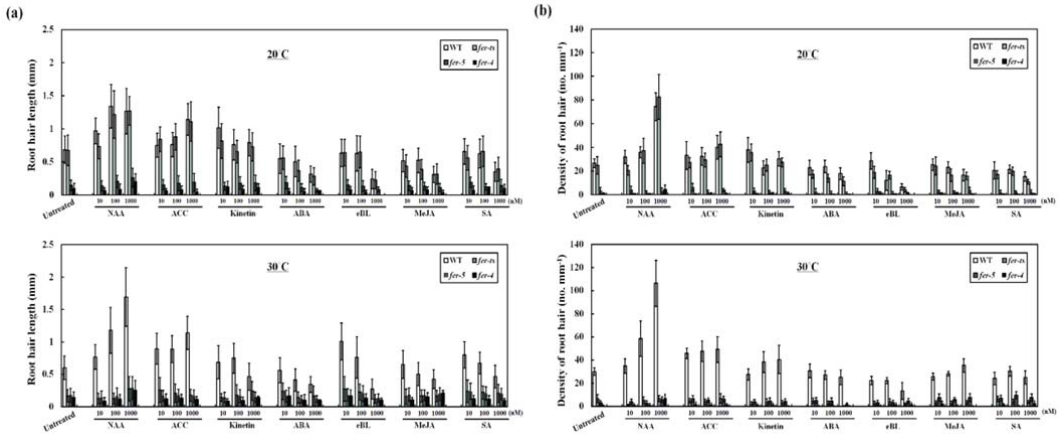

Figure 9. In non-permissive temperatures, *fer-ts* responds to hormone treatments similarly to *fer-4* and *fer-5* mutants.
(a and b) Quantification of root hair length and density in permissive (upper panels) and non-permissive temperature (lower panels) in 10, 100, and 1000 uM concentrations for each of the various hormone treatments (NAA; Auxin, ACC; ethylene, Kinetin; Cytokinin, ABA; Abscisic acid, eBL; epi-brassinosteroid, MeJA; methyl jasmonic acid, SA; Salicylic acid). Three-day-old seedlings were transferred into 1/2 MS liquid media containing three different concentrations of the indicated hormones. Then, transferred plants were incubated at 20°C and 30°C for seven days before quantification. The root hairs were photographed by Olympus AX-70 microscope and root hair length and densities were determined by image J (1.44 version). Error bars represent SD.

different concentrations of hormones, and then root hair lengths and densities were measured either at 20°C or 30°C. Root hair lengths and densities displayed the similar patterns for both wild-type and *fer-ts* at 20°C, while both *fer-4* and *fer-5* root hairs were consistently shorter and less dense (Figure 9a and 9b; upper panels). However at 30°C, *fer-ts* root hair lengths and densities largely resembled the *fer-4* and *fer-5* phenotypes (Figure 9a and 9b; lower panels). Primary root length, total lateral root number, fresh weight, and total leaf numbers of *fer-ts* mutants also displayed a similar temperature-dependent trend; resembling wild-type plants with various hormone treatments at 20°C, but resembling *fer-4* and *fer-5* mutants at 30°C (See supplemental Figure S6).

The *fer-ts* G41S mutation reveals a functionally important role for this highly conserved glycine residue in CrRLK1L subfamily proteins

The profound effects of the G41S substitution of the *fer-ts* mutant on FER protein stability, RALF1 perception, ROS accumulation, and responses to a variety of hormones, suggested this mutation rapidly inactivates *FER* signaling at non-permissive

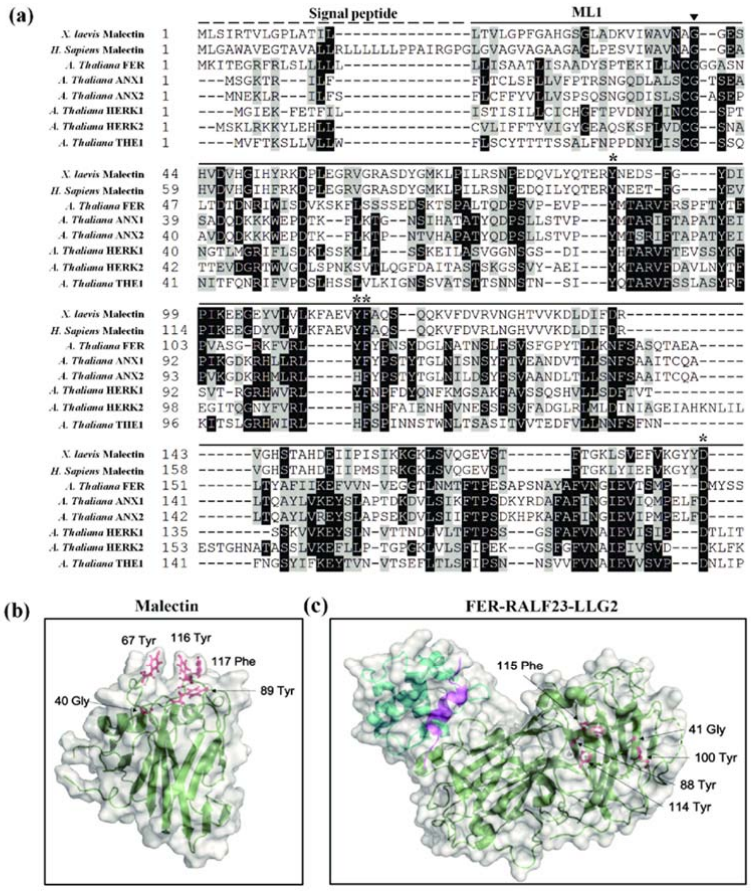

Figure 10. Localization of the highly conserved glycine mutation in *fer-ts* in *A. thaliana* FERONIA:RALF23:LLG2 and *X. laevis* malectin structures.

(a)Several residues important for binding carbohydrate ligands are conserved in plant CrRLK1L receptor kinase family members. Sequences analyzed include animal Malectin (*X. laevis* and *H. sapiens*) FERONIA and other well-characterized CrRLK1L homologs in *A. thaliana* (ANXUR1; ANX1, ANXUR1; ANX2, HERCULES1; HERK1 and THESEUS1; THE1). Putative N-terminal signal peptides are indicated as black dashed lines, and malectin and CrRLK1L ML1 domains by solid lines, respectively. The highly conserved G41 of FER is marked by arrowhead. Black boxes indicate fully conserved residues; shaded boxes indicate similar and partially conserved residues. Conserved residues that have been shown to participate in binding nigerose in the *X.laevis* malectin structure are marked by asterisks. Sequence alignment analysis was performed by CLUSTAL Omega program (http://www.ebi.ac.uk/Tools/msa/clustalo/) and displayed by using BOXSHADE software (www.ch.embnet.org/software/BOX_form.html). (b) Crystal structure of the *X. laevis* malectin protein (PDB ID: 2K46) with binding pocket aromatic residues and the highly conserved glycine residue based on sequence similarity to FER shown in red. (c) Crystal structure of FER protein (green) in complex with RALF23 ligand (magenta) and GPI-anchored protein LLG2 (blue) (PDB ID: 6A5E). No analogous binding pocket is observed on the ML1 domain, as all conserved aromatic residues (red) are buried within the protein. Both (b and c) were generated using PyMol (DeLano Scientific).

365 temperatures. In addition, a similar G37D mutation is responsible for inactivation of
366 THE1, another member of the CrRLK1L family (Hematy et al., 2007), and multiple
367 sequence alignment analysis with other Arabidopsis CrRLK1L family members and
368 animal malectin sequences showed that the G41 residue of FERONIA is absolutely

conserved in these malectins and malectin-like 1 (ML1) domains (Figure 10a, and Supplemental Figure S7). Interestingly, based on structural studies of animal malectin proteins, five key residues (Y67, Y89, Y116, F117, D186; Figure 10b, red residues) were found to form contacts with a bound disaccharide ligand, nigerose, in the active site as determined by structural analysis of the *X. laevis* malectin protein (Schallus et al., 2008; Muller et al., 2010). In this malectin structure these surface exposed residues extend from the malectin fold forming the nigerose binding pocket, with the conserved glycine (G40) the bottom of this structural region (Figure 10b). While several of the tyrosine and phenylalanine residues shown to be important for interaction with carbohydrates in animal malectin proteins are maintained in plant malectin-like domains (e.g. FERONIA Y88, Y114, F115, D197) (Figure 10a, and Supplemental Figure S7), these are not surface exposed in the ML1 domain of the recently described crystal structure of FER (Figure 10c, in green) with its co-receptor LLG2 (Figure 10b, in blue) and a RALF23 ligand (Figure 10c, in magenta) (Xiao et al., 2019). It is however notable that in this structure the invariant glycine (G41; Figure 10c, red residue) of the FER ML1 domain is structurally remote from the RALF23 and LLG2 binding surfaces in the ML2 domain.

DISCUSSION

In eukaryotes, receptor like kinases (RLKs) have been implicated to play an important role in many crucial eukaryotic cellular processes, such as cell cycle progression, cell signaling, embryogenesis, abiotic and biotic stress responses (Shiu and Bleecker, 2001; Morillo and Tax, 2006; Lehti-Shiu et al., 2009). In this study, we isolated and identified a temperature-sensitive root hair elongation mutant, which we have determined is a new mutant *FER* allele that we have called *fer-ts*. The *fer-ts* mutant displays normal overall growth characteristics at permissive temperature (20˚C), but root hair initiation and elongation are specifically and rapidly inhibited within approximately five minutes upon transfer of these plants to non-permissive temperature (30˚C). We have shown that the *fer-ts* mutant is the result of a substitution mutation in which a highly conserved glycine residue in the FER extracellular domain is changed to serine (G41S). FERONIA is a member of the CrRLK1L subfamily of receptor-like kinases (RLKs) in *Arabidopsis* and the mutated glycine residue (G41S) is highly conserved in multiple members of the CrRLK1L family of receptor proteins as well as in animal malectin proteins.

While both FER(WT)-EYFP and FER(G41S)-EYFP fusion proteins displayed a plasma membrane localization at both permissive and non-permissive temperatures, FER(G41S)-EYFP displayed significantly increased protein turnover 30^{o}C (Figure 6), that might be consistent with protein misfolding. Increased accumulation of the FER(G41S)-EYFP in internal membranes upon extended incubation at non-permissive temperatures would be consistent with at least some of the FER(G41S)-EYFP protein being retained in the ER due to misfolding (Supplemental Figure S5). However, this increased protein turnover did not appear to result in loss of accumulation of FER(G41S)-EYFP in plasma membranes. This is likely due to continued protein

412 synthesis and at least some secretion of these proteins at the non-permissive temperature.
413 These results, along with the rapid cessation of root hair elongation (<5 min) in non-
414 permissive temperatures would be consistent with rapid inactivation of FER signaling
415 activity due to protein inactivation rather than simply depletion of FER activity from the
416 plasma membrane due to increased turnover.

417 *FER* has been implicated in a variety of plant processes, including roles in root
418 hair tip growth as well as crucial plant processes, such as pollen tube reception,
419 hypocotyl elongation, regulation of ABA signaling and controlling seed size (Escobar-
420 Restrepo et al., 2007; Deslauriers and Larsen, 2010; Duan et al., 2010; Yu et al., 2012;
421 Yu et al., 2014). In many of these processes, FER signaling appears to regulate ROS
422 production. In constitutive *fer* mutants, ROS levels are reduced, and FER
423 overexpression results in increased ROS levels. The observation that the *fer-ts* mutant
424 also displays reduced ROS levels only at non-permissive temperatures suggests that this
425 mutation affects FER signaling in a similar fashion as other *fer* mutants, perhaps
426 providing a powerful tool for elucidation of downstream signaling events associated
427 with FER function, and indicating that at least one important downstream effect of *FER*
428 signal transduction is regulation of ROS production. This was elegantly explained by
429 the discovery that FER recruits ROPGEFs, which in turn activate ROP GTPases,
430 leading to the stimulation of RHD2 NADPH oxidase dependent ROS production (Duan
431 et al., 2010). Therefore, FER mediated regulation of ROS production is likely important
432 and tightly controlled for many cellular functions.

433 Based on sequence comparison, the extracellular domains of members of the
434 CrRLK1L subfamily of plant RLK proteins might be predicted to share some structural
435 similarity to the mammalian malectin protein (Schallus et al., 2008). Malectin was first

identified and characterized in *X. laevis* as carbohydrate binding protein of the endoplasmic reticulum where it plays an important role in the early steps of protein N-glycosylation for biogenesis of glycoproteins (Schallus et al., 2008). Based on NMR structure analysis, there are five key residues in the malectin domain (Y67, Y89, Y116, F117, D186) that are located in pocket-shaped structure and these aromatic residues and the aspartate mediate interactions with the glucose residues of maltose and nigerose di-saccharide ligands (Schallus et al., 2008). In plants, malectin-like domains are mainly found in CrRLK1L subfamily with a low overall sequence identity with animal malectins (Shiu and Bleecker, 2003). In FER, two malectin-like domains, ML1 and ML2, are found as a tandem-repeat in the extracellular domain. Interestingly, several key residues found in the ligand-binding pocket of the animal malectin structure are maintained in the malectin-like domains of FER and other plant CrRLK1L family members (Schallus et al., 2008). However, the discovery that members of a family of small secreted peptides, RALFs, rather than cell wall polysaccharides or oligosaccharides, serve as important ligands for FER and other CrRLK1L family receptors (Haruta et al., 2014; Ge et al., 2017; Stegmann et al., 2017; Gonneau et al., 2018) might indicate that these extracellular domains may interact with ligands in a manner distinct from their animal counterparts. Indeed the recent structural characterization of ANX1/2 extracellular domains (Du et al., 2018) and the FER extracellular domain in complex with RALF23 and the FER co-receptor, LLG2 (Xiao et al., 2019) has shown that the RALF23 binding domain and interaction with LLG2 occurs primarily with the ML2 domain, and that conserved tyrosine and phenylalanine residues in CrRLK1L malectin folds in these structures appear to be buried within the ML1 fold, and therefore likely unavailable to interact with cell wall carbohydrates in a

460 manner similar to animal malectins.

461 On the other hand, analysis of the animal and plant malectin domains, reveals an
462 additional invariant glycine residue, that is present in all animal and plant malectin
463 sequences, and which is also found in close proximity to pocket-shape ligand-binding
464 cleft determined in the structure of the animal ML1 domain. This invariant glycine is
465 replaced with a serine (G41S) in the *fer-ts* mutation described in this paper. The highly
466 conserved nature of this glycine residue, and the rapid elimination of FER signaling at
467 non-permissive temperatures, suggests a critical role for the FER ML1 domain in ligand
468 binding or transduction of a ligand-binding signal in members of the CrRLK1L family
469 of receptor-like kinases. Indeed, mutation of an analogous glycine residue to aspartic
470 acid (G37D) in the extracellular domain of THESEUS in the *the1-1* mutant also results
471 in a loss of function mutation in this RLK (Hematy et al., 2007). The *the1-1* mutation
472 also results in its insensitivity to its specific RALF ligand, RALF34 (Gonneau et al.,
473 2018). Similarly, the response of *fer-ts* mutant to treatment with RALF1 peptide was
474 dramatically reduced under non-permissive temperature conditions (Figure 7). Precisely
475 how the G41S *fer-ts* mutation, which is structurally distant from the RALF23 peptide
476 binding surface in the FER ML2 domain, would directly block RALF peptide
477 perception and signaling is unclear. One potential explanation may involve the recent
478 discovery of links between *FER* signaling and pectin dynamics during salt stress (Chen
479 et al., 2016; Feng et al., 2018) and fertilization events (Duan et al., 2020). During salt
480 stress, *FER* appears to sense cell wall softening and both FER ML1 and FER ML2
481 domains were shown to directly interact with pectin *in vitro* (Feng et al., 2018). More
482 recently, *FER* function was shown to be required in order to maintain de-esterified
483 pectin levels in the filiform apparatus during pollination and fertilization events (Duan

et al., 2020), Whether the G41S mutation in *fer-ts*, or other analogous mutations of this invariant glycine residue in other CrRLK1L receptors affect the ability of these receptors to interact with or regulate pectin dynamics in plant cell walls is an intriguing possibility that warrants future investigation.

EXPERIMENTAL PROCEDURES

Plant materials and growth conditions

Arabidopsis thaliana ecotype Columbia (Col-0), the *fer-ts* mutant was isolated from an EMS mutagenized population of wild-type (Col-0) stably transformed with a single copy of EYFP-RabAb4 driven by a 35S promoter (Preuss et al., 2004; Weigel and Glazebrook, 2006), and two FERONIA T-DNA insertional mutants (designated as *fer-ts* and two T-DNA insertion mutants, *GABI-GK106A06* (designated as *fer-4*) and *SALK_029056c* (designated as *fer-5*) (Duan et al., 2010) were used in this study. Seeds were sterilized by soaking in 1% bleach solution for 10 min; after washing five times with sterilized water, they were sown onto agar plates for germination. Five- to seven-day-old *A. thaliana* seedlings used in the root-hair growth assays were grown vertically on plates containing 0.25x Murashige and Skoog (Sigma-Aldrich) medium at pH 5.7 supplemented with 0.6% (w/v) phytagel at 20˚C under long day conditions (16 h light/8 h dark cycle). For harvesting seeds, seedling plants were transferred to soil and grown to maturity at 20^{o}C under long day conditions.

Quantification of root hair elongation in *fer-ts* under permissive and non-permissive temperatures

To characterize root hair growth defective phenotypes in the *fer-ts* mutant, bright-field

508 microscopy was carried out using a Nikon Eclipse E600 wide-field microscope with a x
509 10 Plan Apo (0.45 NA) lens as previously described in (Preuss et al., 2004). The *fer-ts*
510 mutants were germinated and grown vertically on plates containing 0.25x MS medium
511 at pH 5.7 supplemented with 0.6% (w/v) phytagel at 20^{o}C for 7 days and then
512 transferred to 30^{o}C and grown for 6 hours before returning back to 20^{o}C growth
513 conditions for an additional 24 hours, when images of roots and root hairs were then
514 collected.Time-lapse video microscopic analysis was carried out under permissive and
515 non-permissive temperature conditions in wild-type and *fer-ts* mutants as described
516 previously [(Preuss et al., 2004)]. Images of growing root hairs were collected every 5 s from
517 seedlings by time-lapse video microscopy. The temperatures of MS medium from
518 permissive to non-permissive temperatures were controlled by an inline single-channel
519 automatic temperature controller (Werner Instruments, Hamden, CT, model:TC-324B)
520 controlled by a dry air thermostat inserted into the growth chamber and situated
521 approximately 2 mm from the ROI. Temperatures were actively recorded using an
522 Infrared Thermometer (Kintrex Inc., Vienna, VA, model:IRT0424). Raw image
523 sequences were cropped with Adobe Photoshop and imported into Fiji-ImageJ
524 (Schindelin et al., 2012) to generate time projections using the Stacks function.
525 Quantification of root-hair lengths, growth rates, and densities were quantified by using
526 calibrate and measure functions.
527
528 **Map-based cloning and full genome sequencing of *fer-ts***
529 Self-fertilized, backcrossed *fer-ts* (ecotype; Columbia) mutants were crossed with
530 Landsberg wild-type plants to generate a mapping population. F_1 crossed plants were
531 checked for heterozygosity with the SSLP marker “nga8” that is polymorphic between

Col-0 and L*er* (Bell and Ecker, 1994). Homozygous *fer-ts* plants were selected from the segregating F2 population by germination on MS media plates at 20°C, and subsequent analysis of root hair tip growth defective phenotypes in non-permissive growth temperatures (30°C). Homozygous plants displaying *fer-ts* phenotypes were grown to maturity at 20°C and seed were collected. Genomic DNA was isolated using Qiagen Plant DNA mini kits, and SSLP markers were used for rough mapping the *fer-ts* mutant lesion, which was initially located on chromosome 3 between the SSLP markers *NIT 1.2* and *NGA6*. Low-resolution mapping narrowed the location of the *fer-ts* mutant locus to an approximately 2 Mb region of chromosome 3, and full genome sequencing was performed to further determine the *fer-ts* mutation within this region. Libraries were generated for both the *fer-ts* and wild-type (ecotype Columbia) extracted DNA using Illumina TruSeq DNA kits and barcoded for multiplexing by the University of Michigan DNA Sequencing Core. Samples were sequenced on an Illumina MiSeq platform with paired-end 150 bp cycles. Sequence reads were checked for quality using FastQC then aligned to the TAIR9 genome using Bowtie2. Potential SNPs were identified using Freebayes. Additional analysis of sequence variants within the low-resolution mapped 2 Mb region of chromosome 3 to eliminate SNPs common to our re-sequenced Col-0 population and the *fer-ts* allele were sorted for context and predicted effect using a custom PERL script.

Fluorescence microscopic analysis

For pFER-FER(WT)-EYFP and pFER-FER(G41S)-EYFP transgenic plants, full-length of *FERONIA* including approximately 2 kb promoter was prepared by PCR reaction and sub cloned into the pCAMBIA-EYFP-C1 expression vector (Preuss et al., 2004). Wild-

556 type and mutant FERONIA sequences were amplified from genomic DNA isolated from
557 wild-type and *fer-ts* mutant plants using PCR. To produce pFER-FER(WT)-EYFP and
558 pFER-FER(G41S)-EYFP transgenic plants, these constructs were introduced into *A.*
559 *tumefaciens* strain GV3101, and *Arabidopsis* plants were transformed with *A.*
560 *tumefaciens* using the 'floral-dip' method (Clough and Bent, 1998). The transgenic
561 plants were selected by germination on 25 mg/L of hygromycin-containing medium
562 (Duchefa, Haarlem, The Netherlands) under long day conditions (16 h light/8 h dark
563 cycle) at 20˚C. Confocal images were generated using a laser confocal microscope
564 (Zeiss Observer.A1) connected to a CSU10 confocal scanner unit (Yokogawa, Japan)
565 and a 10x Plan-Neofluar (0.3 NA lens), 40x Plan-Apochromat (1.3 NA lens) or 100x
566 Plan-Apochromat (1.46 NA lens) oil objective with 491 nm laser excitation and a 535
567 nm emission filter for EGFP and EYFP fluorescence. Images were collected with a
568 Hamamatsu C9100-50 camera operated using the Volocity software version 5 (the
569 electron-multiplying (EM)-CCD detector gain settings were 123, 116 and 190 for
570 images collected with x10, x40 and x100 objectives, respectively). Time-lapse
571 fluorescent images were taken every 5 s using temperature controlled chambers (DeBolt
572 et al., 2007).
573
574 **RT-PCR analysis**
575 For detection of *FERONIA* expression in wild-type, *fer-4*, *fer-5* and *fer-ts* plants, plants
576 frozen immediately in liquid nitrogen. Two microgram aliquots of total RNA extracted
577 from the wild-type or mutant seedlings were used for reverse transcription primed by
578 oligo(dT). Superscript III (Invitrogen, USA) was used for the reverse transcription
579 reaction according to the manufacturer's instructions. One microliter aliquot of the

reaction mixture was used for subsequent PCR analysis. *Actin* was used as a quantifying control.

Detection of ROS in root

ROS detection by using H_2DCF-DA in root hair and primary root was performed following the protocol described previously (Duan et al., 2014). Briefly, Arabidopsis seedlings were germinated grown vertically on 1/4x MS media plates for seven days at permissive (20^{o}C) or non-permissive (30^{o}C) temperatures. Plates were bathed with five ml of 50 uM in H_2DCF-DA (Sigma-Aldrich) suspended in 1/4xMS liquid media for 5 min, followed by two gentle washes with 10 ml of 1/4xMS. Fluorescence images were collected with a Zeiss Axio Imager Z1 fluorescence microscope with 2.5x objective and green (GFP) filter set.

Effect of RALF1 peptide for root growth inhibition in *fer-ts* mutant

Synthetic Arabidopsis RALF1 polypeptide was synthesized by using 9-fluorenylmethyl chloroformate solid-phase chemistry with a peptide synthesizer from Thermo Scientific company and confirmed by MALD-TOF analysis (Applied Biosystems Voyager System 2098, USA). After synthesis, 5 mg of reduced synthetic polypeptide was oxidized by dissolving in 25 ml of degassed 0.1 M ammonium bicarbonate and incubating for 2 days in an opened flask under 4˚C, then lyophilized. Lyophilized RALF1 powder was re-suspended in 10 ml of PBS buffer followed by two buffer exchange steps using Amicon Ultra centrifugal filter (Ultracel-3K, 3000g for 45 min each) to remove any residual ammonium bicarbonate. Seedling germination was performed in 1/2x MS liquid

603 medium at 20°C for 3 days in long-day conditions (16-h days with 150 $\mu E \cdot m^{-2} \cdot s^{-1}$ (E,
604 Einstein; 1 E = 1 mol of photons) light intensity. After 3 days, germinated Arabidopsis
605 seeds were transferred to 6 well Falcon tissue culture plate with 3 ml of 1/2xMS liquid
606 media containing 1 μM RALF1 or an equal volume of PBS and agitated on a shaker at
607 100 rpm (Model VS2010, Vision Scientific CO.,LTD) for an additional 3 days at 20°C
608 or 30°C. All solutions were filter-sterilized (0.2 μm pores, Minisart 16534), and the
609 seedlings were photographed 3 days after being transferred to the media. Quantification
610 of primary root length was measured using ImageJ software.
611
612 **Accession numbers**
613 Sequences of the genes in this paper may be found in the GeneBank/EMBL database
614 library under the following accession numbers: At3g51550 (FER), At4g39990
615 (RabA4b), At3g18780 (Actin2), At3g04690 (ANX1), At5g28680 (ANX2), At3g46290
616 (HERK1), At1g30570 (HERK2), At5g54380 (THE1), NP_001085212.1 (*X. laevis*
617 Malectin), NP_055545.1 (*H. sapiens* Malectin).
618

619 ## ACKNOWLEDGEMENTS
620 We thank to Dr. Hen-Ming Wu and Dr. Alice Cheung (University of Massachusetts) for
621 providing *fer-4* and *fer-5* mutants, and Jiyuan Yang for assistance in assembling and
622 editing the manuscript. This research was supported by the U.S. Department of Energy
623 Office of Science, Office of Basic Energy Sciences, Physical Biosciences program (DE-
624 FG02-07ER15887; S.P., F.G., J.C., and E.N,), the National Science Foundation under
625 Grant No. 1817697 (A.A., H.M, and E.N.), and the BK21plus program of the Ministry
626 of Education, Science and Technology in Korea (D.K., and J-D.B.). This work used the

Extreme Science and Engineering Discovery Environment (XSEDE; (John W Towns, 2014), which is supported by National Science Foundation grant number ACI-1548562.

FIGURE LEGENDS

Figure 1. Isolation of a temperature-sensitive root hair growth defect mutant.

(a) Seven day-old seedling plants were grown vertically in 1/4 MS media under 20˚C and transferred to 30˚C for 6 h, followed by 24 h recovery at 20°C. Bright field images were collected with a Nikon Eclipse E600 wide-field microscope with a 20x Plan Apo DIC (0.75 NA) lens. Dashed lines indicate root tip positions when seedling plants were transferred to 30˚C condition for 6 hours, and again when they were transferred back to 20˚C. Scale bars = 200 µm. (b) Localization of EYFP-RabA4b protein in growing root-hair cells of *fer-ts* mutants at 20˚C and 30˚C. Medial root hair sections were collected using spinning-disk confocal microscopy from growing root-hair cells of seven-day-old seedlings stably expressing EYFP-RabA4b in the *fer-ts* mutant in 20°C (left) or 30°C (right) using a Zeiss 40x Plan-Apochromat (1.3 NA) lens and appropriate EYFP fluorescence filter sets. Scale bars = 10 µm. Insets, magnified images to show details of EYFP-RabA4b subcellular localization in root-hair tips. Scale bars = 2 µm. (c) Quantification of root hair length in WT and *fer-ts* mutants under 20˚C (wild-type (n=392), *fer-ts* (n=454)) and 30˚C (wild-type (n=185), *fer-ts* (n=23)) conditions. (d) Calculation of root hair densities in WT and *fer-ts* mutants at 20˚C (wild-type (n=392), *fer-ts* (n=454)) and 30˚C (wild-type (n=185), *fer-ts* (n=23)) in fully expanded primary roots of seven-day old plants. In each case, root hair lengths and densities were measured from n=20 individual seedlings. Error bars represent SD. **p<0.001 by

Student's *t*-test.

Figure 2. Root hair growth dynamics in WT and *fer-ts* seedlings.

(a) Root hair tip-growth in WT and *fer-ts* mutant plants under permissive (20°C) and non-permissive (30°C) temperatures by time-lapse microscopy. Bright field images of growing root hairs of WT and *fer-ts* mutant plants were collected every minute by time-lapse microscopy using a Zeiss 40x Plan-Apochromat (1.3 NA) lens. Representative images of WT and *fer-ts* mutant root hair elongation are presented at 10 min intervals. (b) Quantitative analysis of WT (n=4) and *fer-ts* mutant (n=4) root hair lengths upon transition to 30˚C. WT (black squares) and *fer-ts* (black triangles) mutant root hair elongation were measured every five minutes and root hair lengths were determined using the measure function in Image J (1.44 version) The dashed line indicates transition from 20°C to 30°C. Error bars represent SD. *$p<0.05$, **$p<0.01$ by Student's *t*-test.

Figure 3. Temperature-sensitive subcellular dynamics of EYFP-RabA4b labeled compartments in growing root hairs in *fer-ts* mutants.

(a) Localization of EYFP-RabA4b protein in growing root-hair cells of *fer-ts* mutant at permissive (20°C) or non-permissive (30°C) temperature conditions. Growing *fer-ts* root hairs were imaged at one minute intervals for 30 min at 20˚C at which the growth chamber temperature was raised to 30˚C. For each time point, both bright field (Bright) and fluorescence (YFP) images were collected sequentially, and tip-localized EYFP-RabA4b compartments were monitored by spinning-disk fluorescence confocal

673 microscopy using a Zeiss 40x Plan-Apochromat (1.3 NA) lens with appropriate EYFP
674 fluorescence filter sets. The dashed line indicates the temperature transition from 20˚C
675 to 30˚C. Merge indicates overlapped images of bright and EYFP fluorescent signals. (b)
676 Monitoring of chamber temperatures of *fer-ts* mutant. Insert, transition of the growth
677 chamber temperature from 20˚C up to 30˚C were measured every 1 min by dry air
678 thermostat situated in close proximity (~2 mm) from the growing root hair. (c)
679 Quantification of root hair elongation and EYFP-RabA4b root hair tip localization. Root
680 hair length and EYFP-RabA4b fluorescence were quantified by Image J (1.44 version)
681 program every 1 min.
682
683 **Figure 4.** Map-based cloning of *fer-ts*.
684 (a) A linear diagram of the Arabidopsis third chromosome is shown, with a magnified
685 F24M12 marker region displayed below. The centromere is indicated with filled-
686 rectangle. Low-resolution map-based cloning resulted in identification of the *fer-ts*
687 locus within an approximately 2 Mb region of chromosome III bounded by markers
688 NIT1.2 and CIW19 (Double headed arrow). (b) SNPs specific to the ts-mutant within
689 this region were identified using whole genomic resequencing, followed by targeted
690 resequencing of genomic DNA sequencing of *fer-ts* and wild-type parental lines. A
691 single G→A substitution was found in *FERONIA* (At3g51550). The arrowhead
692 indicates G121A substituted mutation in *FERONIA* gene locus. (c) Schematic diagram
693 of FERONIA protein domains and mutation regions, composed of an N-terminal
694 extracellular domain (tandem repeat malectin-like domains; ML1 and ML2), TM
695 (transmembrane) domain in the middle region and a C-terminal kinase domain
696 (serine/threonine kinase), end of N-terminus has signal peptide (SP) sequence for

plasma-membrane trafficking. The *fer-4* and *fer-5* mutants displayed that T-DNA was inserted in malectin-like domain 1 and kinase domain, respectively. (d) RT-PCR analysis of T-DNA inserted mutants and EMS mutants. FER (K) and FER (ExDo) was amplified using pair of P1 and P2 primers and P3 and P4 primers, respectively. Actin was used as a loading control.

Figure 5. The *fer-ts* mutant confers ts-root hair growth defects when crossed with *fer-4* and *fer-5* mutants.

(a) Wild-type (WT), *fer-4, fer-5*, and F1 progeny from crosses (paternal = *fer-ts*, maternal = *fer-4* or *fer-5*) of *fer-ts/fer-4* and *fer-ts/fer-5* were grown vertically for seven days at 20^{o}C, transferred to 30^{o}C for 6 h, and then grown for an additional 24 h at 20^{o}C. Bright field images were collected with a Nikon Eclipse E600 wide-field microscope with a 20x Plan Apo DIC (0.75 NA) lens. Both *fer-ts/fer-4* and *fer-ts/fer-5* progeny clearly demonstrated a ts-dependent root hair phenotype. Scale bars = 200 µm. (b) Schematic diagram of the *FERONIA* gene structure. Open and filled boxes indicate untranslated regions (UTRs) and exon regions, respectively. The locations of T-DNA insertion mutants (*fer-4* and *fer-5*) and *fer-ts* are indicated by triangles and arrows, respectively. (c) Genotyping of crossed F1 plants. Genomic DNA was extracted from F1 generation plants and subjected PCR to confirm presence of the *fer-4* and *fer-5* genotypes (d) Both *fer-4* and *fer-5* display temperature-dependent root hair phenotypes when transformed with a fluorescently-tagged FER construct containing the *fer-ts* mutation (pFER-FER(G41S)-EYFP). Seven-day old seedlings were grown vertically for seven days at 20^{o}C, transferred to 30^{o}C for 6 h, and then grown for an additional 24 h at

720 20°C. Bright field images were collected with a Nikon Eclipse E600 wide-field
721 microscope with a 20x Plan Apo DIC (0.75 NA) lens. Presence of the transgenic pFER-
722 FER(G41S)-EYFP construct clearly demonstrated a ts-dependent root hair phenotype.
723 Scale bars = 200 μm.
724
725 **Figure 6.** Subcellular localization of FER(WT)-EYFP and FER(G41S)-EYFP
726 fluorescent fusion proteins in stably transformed *Arabidopsis*.
727 (a) Subcellular localization of FER(WT)-EYFP protein in various tissues. Fluorescent
728 confocal images displaying the subcellular distribution of FER(WT)-EYFP protein was
729 detected from growing root, leaf and root hair cells of seven-day-old seedlings in *pFER-*
730 *FER(WT)-EYFP*/WT transgenic plants. Cell walls were counter-stained by incubating
731 for 5 min in a propidium iodide (PI) solution (10 μg/ml). Images were collected by
732 spinning-disk fluorescence confocal microscopy using a Zeiss 40x Plan-Apochromat
733 (1.3 NA) lens with appropriate EYFP and PI fluorescence filter sets. Scale bars = 20 μm.
734 (b) Magnified images of FER(WT)-EYFP fluorescence. FER(WT)-EYFP in wild-type
735 of growing root cells of seven-day-old *A. thaliana* seedlings was detected by spinning-
736 disc confocal microscopy using a Zeiss 100x Plan-Apochromat (1.46 NA) oil
737 immersion objective with appropriate EYFP and PI filter sets. Scale bars = 10 μm. (c)
738 Protein turnover rates of FER(WT)-EYFP and FER(G41S)-EYFP at non-permissive
739 temperature (30°C). Five-day old seedling were grown at 20°C and then treated with
740 200 μM cycloheximide and transferred to 30°C. Total proteins were extracted at each
741 time point and the relative levels were determined using immunoblotting with anti-GFP
742 and anti-actin antibodies. FER(G41S)-EYFP levels rapidly decreased during the time
743 course, while levels of FER(WT)-EYFP were not significantly reduced. Actin was used

744 as a loading control. (d-e) Subcellular localization of FER(WT)-EYFP (d) and
745 FER(G41S)-EYFP (e) fluorescent fusions in root and root hair cells at permissive (20°C)
746 and non-permissive (30°C) temperatures. Cells were counterstained with FM4-64 to
747 visualize cell walls. Images were collected by spinning-disk fluorescence confocal
748 microscopy using a Zeiss 40x Plan-Apochromat (1.3 NA) lens with appropriate EYFP
749 and FM4-64 fluorescence filter sets. Scale bars = 20 µm; root, 10 µm; root hair.
750
751 **Figure 7**. *fer-ts* mutants are partially insensitive to RALF1 peptide mediated root
752 growth inhibition at non-permissive temperatures.
753 Wild-type (WT), *fer-ts*, or *fer-5* plants were germinated and grown for 3 days in ½ MS
754 liquid media at 20°C, and then transferred to ½ MS liquid media containing 1uM
755 RALF1 peptide (RALF+) or a mock buffer control (RALF-) and grown an additional 3
756 days at 20°C (a) or 30°C (b). Images of representative seedlings were collected using an
757 Olympus SZX12 stereoscopic microscope. Quantification of primary root lengths (n =
758 10 seedlings) in the presence or absence of RALF1 peptide treatment in permissive,
759 20˚C (c) and non-permissive, 30˚C (d) conditions. Primary root lengths were
760 determined using Image J. Error bars represent SD. *p<0.05, **p<0.01 by Student's *t*-
761 test.
762
763 **Figure 8.** Detection of ROS in WT, *fer-ts* and *fer-5* primary roots and root hairs.
764 (a) ROS accumulation in permissive and non-permissive temperature conditions with or
765 without auxin treatments. Wild-type (WT), *fer-ts*, *fer-4*, or *fer-5* seedlings were grown
766 vertically on ¼ MS media plates for seven days at permissive (20°C) or non-permissive
767 (30°C) temperatures in the presence or absence of (10 nM NAA). Plates were bathed

768 with five ml of 50 uM in H_2DCF-DA suspended in ¼ MS liquid media for 5 min,
769 followed by two gentle washes with 10 ml of ¼ MS. Fluorescence images were
770 collected with a Zeiss Axio Imager Z1 fluorescence microscope with 2.5x objective and
771 green (GFP) filter set. The WT ROS image was acquired by auto-exposure, all other
772 images were acquired using the WT exposure conditions. Scale bars = 500 µm. (b) The
773 rectangle in (a) indicates a representative region of interest (ROI) where average ROS
774 intensity was quantified for the samples. Intensities of ROS were quantified by image J
775 program. Error bars represent SD. **p<0.01 by Student's *t*-test.
776
777 **Figure 9.** In non-permissive temperatures, *fer-ts* responds to hormone treatments
778 similarly to *fer-4* and *fer-5* mutants.
779 (a and b) Quantification of root hair length and density in permissive (upper panels) and
780 non-permissive temperature (lower panels) in 10, 100, and 1000 uM concentrations for
781 each of the various hormone treatments (NAA; Auxin, ACC; ethylene, Kinetin;
782 Cytokinin, ABA; Abscisic acid, eBL; epi-brassinosteroid, MeJA; methyl jasmonic acid,
783 SA; Salicylic acid). Three-day-old seedlings were transferred into ½ MS liquid media
784 containing three different concentrations of the various hormones. Then, transferred
785 plants were incubated at 20˚C and 30˚C for seven days before quantification. The root
786 hairs were photographed by Olympus AX-70 microscope and root hair length and
787 densities were determined by image J (1.44 version). Error bars represent SD.
788
789 **Figure 10.** Localization of the highly conserved glycine mutation in fer-ts in *A. thaliana*
790 FERONIA:RALF23:LLG2 and *X. laevis* malectin structures.
791 (a)Several residues important for binding carbohydrate ligands are conserved in plant

792 CrRLK1L receptor kinase family members. Sequences analyzed include animal
793 Malectin (*X. laevis* and *H. sapiens*) FERONIA and other well-characterized CrRLK1L
794 homologs in *A. thaliana* (ANXUR1; ANX1, ANXUR1; ANX2, HERCULES1; HERK1
795 and THESEUS1; THE1). Putative N-terminal signal peptides are indicated as black
796 dashed lines, and malectin and CrRLK1L ML1 domains by solid lines, respectively. The
797 highly conserved G41 of FER is marked by arrowhead. Black boxes indicate fully
798 conserved residues; shaded boxes indicate similar and partially conserved residues.
799 Conserved residues that have been shown to participate in binding nigerose in the
800 *X.laevis* malectin structure are marked by asterisks. Sequence alignment analysis was
801 performed by CLUSTAL Omega program (http://www.ebi.ac.uk/Tools/msa/clustalo/)
802 and displayed by using BOXSHADE software
803 (www.ch.embnet.org/software/BOX_form.html). (b) Crystal structure of the *X. laevis*
804 malectin protein (PDB ID: 2K46) with binding pocket aromatic residues and the highly
805 conserved glycine residue based on sequence similarity to FER shown in red. (c)
806 Crystal structure of FER protein (green) in complex with RALF23 ligand (magenta) and
807 GPI-anchored protein LLG2 (blue) (PDB ID: 6A5E). No analogous binding pocket is
808 observed on the ML1 domain, as all conserved aromatic residues (red) are buried within
809 the protein. Both (b and c) were generated using PyMol (DeLano Scientific).
810

811 ## SUPPORTING INFORMATION

812 Additional supporting Information may be found in the online version of this article.
813 **Figure S1.** Primary root growth of *fer-ts* mutants under permissive and non-permissive
814 temperature conditions.

Figure S2. Subcellular dynamics of EYFP-RabA4b labeled compartments in growing root hairs in wild-type plants in permissive and non-permissive temperature conditions.

Figure S3. Confirmation of *fer-ts* phenotype by crossing with *fer-4* and *fer-5* mutant.

Figure S4. Complementation of *fer-ts* mutant by pFER::FER(WT)-EYFP.

Figure S5. Subcellular localization of pFER::FER(G41S)-EYFP grown in extended on-permissive temperature conditions.

Figure S6. Sequence alignment of *Arabidopsis* CrRLK1L subfamily receptor kinases.

Figure S7. Hormonal effects on primary root length, total lateral root number, fresh weight and total leaf number in permissive and non-permissive temperature conditions.

Movie S1. Time-lapse imaging of growing root hairs of wild-type and *ltl2* mutant in permissive and non-permissive temperatures

Movie S2. Dynamics of EYFP fused FERONIA protein localization in growing root hairs.

Movies S3 and S4. FER(WT)-EYFP and FER(G41S)-EYFP protein localization in growing primary roots in permissive and non-permissive temperature conditions.

Table S1. List of primers used in this study.

Parsed Citations

Bell CJ, Ecker JR (1994) Assignment of 30 microsatellite loci to the linkage map of Arabidopsis. Genomics 19: 137-144
Pubmed: Author and Title
Google Scholar: Author Only Title Only Author and Title

Boisson-Dernier A, Roy S, Kritsas K, Grobei MA, Jaciubek M, Schroeder JI, Grossniklaus U (2009) Disruption of the pollen-expressed FERONIA homologs ANXUR1 and ANXUR2 triggers pollen tube discharge. Development 136: 3279-3288
Pubmed: Author and Title
Google Scholar: Author Only Title Only Author and Title

Carol RJ, Dolan L (2006) The role of reactive oxygen species in cell growth: lessons from root hairs. J Exp Bot 57: 1829-1834
Pubmed: Author and Title
Google Scholar: Author Only Title Only Author and Title

Chen J, Yu F, Liu Y, Du C, Li X, Zhu S, Wang X, Lan W, Rodriguez PL, Liu X, Li D, Chen L, Luan S (2016) FERONIA interacts with ABI2-type phosphatases to facilitate signaling cross-talk between abscisic acid and RALF peptide in Arabidopsis. Proc Natl Acad Sci U S A 113: E5519-5527
Pubmed: Author and Title
Google Scholar: Author Only Title Only Author and Title

Cheung AY, Wu HM (2011) THESEUS 1, FERONIA and relatives: a family of cell wall-sensing receptor kinases? Curr Opin Plant Biol 14: 632-641
Pubmed: Author and Title
Google Scholar: Author Only Title Only Author and Title

Cho HT, Cosgrove DJ (2002) Regulation of root hair initiation and expansin gene expression in Arabidopsis. Plant Cell 14: 3237-3253
Pubmed: Author and Title
Google Scholar: Author Only Title Only Author and Title

Clough SJ, Bent AF (1998) Floral dip: a simplified method for Agrobacterium-mediated transformation of Arabidopsis thaliana. Plant J 16: 735-743
Pubmed: Author and Title
Google Scholar: Author Only Title Only Author and Title

Cole RA, Fowler JE (2006) Polarized growth: maintaining focus on the tip. Curr Opin Plant Biol 9: 579-588
Pubmed: Author and Title
Google Scholar: Author Only Title Only Author and Title

DeBolt S, Gutierrez R, Ehrhardt DW, Somerville C (2007) Nonmotile cellulose synthase subunits repeatedly accumulate within localized regions at the plasma membrane in Arabidopsis hypocotyl cells following 2,6-dichlorobenzonitrile treatment. Plant Physiol 145: 334-338
Pubmed: Author and Title
Google Scholar: Author Only Title Only Author and Title

Deslauriers SD, Larsen PB (2010) FERONIA is a key modulator of brassinosteroid and ethylene responsiveness in Arabidopsis hypocotyls. Mol Plant 3: 626-640
Pubmed: Author and Title
Google Scholar: Author Only Title Only Author and Title

Du S, Qu LJ, Xiao J (2018) Crystal structures of the extracellular domains of the CrRLK1L receptor-like kinases ANXUR1 and ANXUR2. Protein Sci 27: 886-892
Pubmed: Author and Title
Google Scholar: Author Only Title Only Author and Title

Duan Q, Kita D, Johnson EA, Aggarwal M, Gates L, Wu HM, Cheung AY (2014) Reactive oxygen species mediate pollen tube rupture to release sperm for fertilization in Arabidopsis. Nat Commun 5: 3129
Pubmed: Author and Title
Google Scholar: Author Only Title Only Author and Title

Duan Q, Kita D, Li C, Cheung AY, Wu HM (2010) FERONIA receptor-like kinase regulates RHO GTPase signaling of root hair development. Proc Natl Acad Sci U S A 107: 17821-17826
Pubmed: Author and Title
Google Scholar: Author Only Title Only Author and Title

Duan Q, Liu MJ, Kita D, Jordan SS, Yeh FJ, Yvon R, Carpenter H, Federico AN, Garcia-Valencia LE, Eyles SJ, Wang CS, Wu HM, Cheung AY (2020) FERONIA controls pectin- and nitric oxide-mediated male-female interaction. Nature 579: 561-566
Pubmed: Author and Title
Google Scholar: Author Only Title Only Author and Title

Escobar-Restrepo JM, Huck N, Kessler S, Gagliardini V, Gheyselinck J, Yang WC, Grossniklaus U (2007) The FERONIA receptor-like kinase mediates male-female interactions during pollen tube reception. Science 317: 656-660
Pubmed: Author and Title
Google Scholar: Author Only Title Only Author and Title

Feng W, Kita D, Peaucelle A, Cartwright HN, Doan V, Duan Q, Liu MC, Maman J, Steinhorst L, Schmitz-Thom I, Yvon R, Kudla J, Wu HM, Cheung AY, Dinneny JR (2018) The FERONIA Receptor Kinase Maintains Cell-Wall Integrity during Salt Stress through Ca(2+) Signaling. Curr Biol 28: 666-675 e665
Pubmed: Author and Title
Google Scholar: Author Only Title Only Author and Title

Feng Y, Press B, Wandinger-Ness A (1995) Rab 7: an important regulator of late endocytic membrane traffic. J Cell Biol 131: 1435-1452
Pubmed: Author and Title
Google Scholar: Author Only Title Only Author and Title

Foreman J, Demidchik V, Bothwell JHF, Mylona P, Miedema H, Torres MA, Linstead P, Costa S, Brownlee C, Jones JDG, Davies JM, Dolan L (2003) Reactive oxygen species produced by NADPH oxidase regulate plant cell growth. Nature 422: 442-446
Pubmed: Author and Title
Google Scholar: Author Only Title Only Author and Title

Ge Z, Bergonci T, Zhao Y, Zou Y, Du S, Liu MC, Luo X, Ruan H, Garcia-Valencia LE, Zhong S, Hou S, Huang Q, Lai L, Moura DS, Gu H, Dong J, Wu HM, Dresselhaus T, Xiao J, Cheung AY, Qu LJ (2017) Arabidopsis pollen tube integrity and sperm release are regulated by RALF-mediated signaling. Science 358: 1596-1600
Pubmed: Author and Title
Google Scholar: Author Only Title Only Author and Title

Gilroy S, Jones DL (2000) Through form to function: root hair development and nutrient uptake. Trends Plant Sci 5: 56-60
Pubmed: Author and Title
Google Scholar: Author Only Title Only Author and Title

Gonneau M, Desprez T, Martin M, Doblas VG, Bacete L, Miart F, Sormani R, Hematy K, Renou J, Landrein B, Murphy E, Van De Cotte B, Vernhettes S, De Smet I, Hofte H (2018) Receptor Kinase THESEUS1 Is a Rapid Alkalinization Factor 34 Receptor in Arabidopsis. Curr Biol 28: 2452-2458 e2454
Pubmed: Author and Title
Google Scholar: Author Only Title Only Author and Title

Greeff C, Roux M, Mundy J, Petersen M (2012) Receptor-like kinase complexes in plant innate immunity. Front Plant Sci 3: 209
Pubmed: Author and Title
Google Scholar: Author Only Title Only Author and Title

Guo H, Li L, Ye H, Yu X, Algreen A, Yin Y (2009) Three related receptor-like kinases are required for optimal cell elongation in Arabidopsis thaliana. Proc Natl Acad Sci U S A 106: 7648-7653
Pubmed: Author and Title
Google Scholar: Author Only Title Only Author and Title

Haruta M, Sabat G, Stecker K, Minkoff BB, Sussman MR (2014) A peptide hormone and its receptor protein kinase regulate plant cell expansion. Science 343: 408-411
Pubmed: Author and Title
Google Scholar: Author Only Title Only Author and Title

Hematy K, Hofte H (2008) Novel receptor kinases involved in growth regulation. Curr Opin Plant Biol 11: 321-328
Pubmed: Author and Title
Google Scholar: Author Only Title Only Author and Title

Hematy K, Sado PE, Van Tuinen A, Rochange S, Desnos T, Balzergue S, Pelletier S, Renou JP, Hofte H (2007) A receptor-like kinase mediates the response of Arabidopsis cells to the inhibition of cellulose synthesis. Curr Biol 17: 922-931
Pubmed: Author and Title
Google Scholar: Author Only Title Only Author and Title

Hepler PK, Vidali L, Cheung AY (2001) Polarized cell growth in higher plants. Annu Rev Cell Dev Biol 17: 159-187
Pubmed: Author and Title
Google Scholar: Author Only Title Only Author and Title

Huang GQ, Li E, Ge FR, Li S, Wang Q, Zhang CQ, Zhang Y (2013) Arabidopsis RopGEF4 and RopGEF10 are important for FERONIA-mediated developmental but not environmental regulation of root hair growth. New Phytol 200: 1089-1101
Pubmed: Author and Title
Google Scholar: Author Only Title Only Author and Title

Huck N, Moore JM, Federer M, Grossniklaus U (2003) The Arabidopsis mutant feronia disrupts the female gametophytic control of pollen tube reception. Development 130: 2149-2159
Pubmed: Author and Title
Google Scholar: Author Only Title Only Author and Title

John W Towns TC, Maytal Dahan, Ian Foster, Kelly Gaither, Andrew Grimshaw, Victor Hazlewood, Scott Lathrop, Dave Lifka, Gregory D. Peterson, Ralph Roskies, J. Ray Scott, Nancy Wilkens-Diehr (2014) XSEDE: Accelerating scientific discovery. Computing in Science and Engineering 16: 62-74
Pubmed: Author and Title
Google Scholar: Author Only Title Only Author and Title

Jones MA, Shen JJ, Fu Y, Li H, Yang Z, Grierson CS (2002) The Arabidopsis Rop2 GTPase is a positive regulator of both root hair initiation and tip growth. Plant Cell 14: 763-776
Pubmed: Author and Title
Google Scholar: Author Only Title Only Author and Title

Lehti-Shiu MD, Zou C, Hanada K, Shiu SH (2009) Evolutionary history and stress regulation of plant receptor-like kinase/pelle genes. Plant Physiol 150: 12-26
Pubmed: Author and Title
Google Scholar: Author Only Title Only Author and Title

Li C, Wu HM, Cheung AY (2016) FERONIA and Her Pals: Functions and Mechanisms. Plant Physiol 171: 2379-2392
Pubmed: Author and Title
Google Scholar: Author Only Title Only Author and Title

Lindner H, Muller LM, Boisson-Dernier A, Grossniklaus U (2012) CrRLK1L receptor-like kinases: not just another brick in the wall. Curr Opin Plant Biol 15: 659-669
Pubmed: Author and Title
Google Scholar: Author Only Title Only Author and Title

Miyazaki S, Murata T, Sakurai-Ozato N, Kubo M, Demura T, Fukuda H, Hasebe M (2009) ANXUR1 and 2, sister genes to FERONIA/SIRENE, are male factors for coordinated fertilization. Curr Biol 19: 1327-1331
Pubmed: Author and Title
Google Scholar: Author Only Title Only Author and Title

Molendijk AJ, Bischoff F, Rajendrakumar CS, Friml J, Braun M, Gilroy S, Palme K (2001) Arabidopsis thaliana Rop GTPases are localized to tips of root hairs and control polar growth. Embo J 20: 2779-2788
Pubmed: Author and Title
Google Scholar: Author Only Title Only Author and Title

Morillo SA, Tax FE (2006) Functional analysis of receptor-like kinases in monocots and dicots. Curr Opin Plant Biol 9: 460-469
Pubmed: Author and Title
Google Scholar: Author Only Title Only Author and Title

Muller LN, Muhle-Goll C, Biskup MB (2010) The Glc2Man2-fragment of the N-glycan precursor--a novel ligand for the glycan-binding protein malectin? Org Biomol Chem 8: 3294-3299
Pubmed: Author and Title
Google Scholar: Author Only Title Only Author and Title

Ngo QA, Vogler H, Lituiev DS, Nestorova A, Grossniklaus U (2014) A calcium dialog mediated by the FERONIA signal transduction pathway controls plant sperm delivery. Dev Cell 29: 491-500
Pubmed: Author and Title
Google Scholar: Author Only Title Only Author and Title

Nielsen E (2008) Plant Cell Wall Biogenesis During Tip Growth in Root Hair Cells. In Plant Cell Monographs, Vol 12. Springer-Verlag, Berlin Heidelberg, pp 85-102
Pubmed: Author and Title
Google Scholar: Author Only Title Only Author and Title

Pearce G, Moura DS, Stratmann J, Ryan CA, Jr. (2001) RALF, a 5-kDa ubiquitous polypeptide in plants, arrests root growth and development. Proc Natl Acad Sci U S A 98: 12843-12847
Pubmed: Author and Title
Google Scholar: Author Only Title Only Author and Title

Preuss ML, Santos-Serna J, Falbel TG, Bednarek SY, Nielsen E (2004) The Arabidopsis Rab GTPase RabA4b Localizes to the Tips of Growing Root Hair Cells. Plant Cell 16: 1589-1603
Pubmed: Author and Title
Google Scholar: Author Only Title Only Author and Title

Preuss ML, Schmitz AJ, Thole JM, Bonner HK, Otegui MS, Nielsen E (2006) A role for the RabA4b effector protein PI-4Kbeta1 in polarized expansion of root hair cells in Arabidopsis thaliana. J Cell Biol 172: 991-998
Pubmed: Author and Title
Google Scholar: Author Only Title Only Author and Title

Rotman N, Rozier F, Boavida L, Dumas C, Berger F, Faure JE (2003) Female control of male gamete delivery during fertilization in Arabidopsis thaliana. Curr Biol 13: 432-436
Pubmed: Author and Title
Google Scholar: Author Only Title Only Author and Title

Schallus T, Jaeckh C, Feher K, Palma AS, Liu Y, Simpson JC, Mackeen M, Stier G, Gibson TJ, Feizi T, Pieler T, Muhle-Goll C (2008) Malectin: a novel carbohydrate-binding protein of the endoplasmic reticulum and a candidate player in the early steps of protein N-glycosylation. Mol Biol Cell 19: 3404-3414
Pubmed: Author and Title
Google Scholar: Author Only Title Only Author and Title

Schindelin J, Arganda-Carreras I, Frise E, Kaynig V, Longair M, Pietzsch T, Preibisch S, Rueden C, Saalfeld S, Schmid B, Tinevez JY,

White DJ, Hartenstein V, Eliceiri K, Tomancak P, Cardona A (2012) Fiji: an open-source platform for biological-image analysis. Nat Methods 9: 676-682
Pubmed: Author and Title
Google Scholar: Author Only Title Only Author and Title

Schulze-Muth P, Irmler S, Schroder G, Schroder J (1996) Novel type of receptor-like protein kinase from a higher plant (Catharanthus roseus). cDNA, gene, intramolecular autophosphorylation, and identification of a threonine important for auto- and substrate phosphorylation. J Biol Chem 271: 26684-26689
Pubmed: Author and Title
Google Scholar: Author Only Title Only Author and Title

Shih HW, Miller ND, Dai C, Spalding EP, Monshausen GB (2014) The receptor-like kinase FERONIA is required for mechanical signal transduction in Arabidopsis seedlings. Curr Biol 24: 1887-1892
Pubmed: Author and Title
Google Scholar: Author Only Title Only Author and Title

Shiu SH, Bleecker AB (2001) Plant receptor-like kinase gene family: diversity, function, and signaling. Sci STKE 2001: re22
Pubmed: Author and Title
Google Scholar: Author Only Title Only Author and Title

Shiu SH, Bleecker AB (2003) Expansion of the receptor-like kinase/Pelle gene family and receptor-like proteins in Arabidopsis. Plant Physiol 132: 530-543
Pubmed: Author and Title
Google Scholar: Author Only Title Only Author and Title

Smith IF, Hitt B, Green KN, Oddo S, LaFerla FM (2005) Enhanced caffeine-induced Ca2+ release in the 3xTg-AD mouse model of Alzheimer's disease. J Neurochem 94: 1711-1718
Pubmed: Author and Title
Google Scholar: Author Only Title Only Author and Title

Stegmann M, Monaghan J, Smakowska-Luzan E, Rovenich H, Lehner A, Holton N, Belkhadir Y, Zipfel C (2017) The receptor kinase FER is a RALF-regulated scaffold controlling plant immune signaling. Science 355: 287-289
Pubmed: Author and Title
Google Scholar: Author Only Title Only Author and Title

Thole JM, Vermeer JE, Zhang Y, Gadella TW, Jr., Nielsen E (2008) Root hair defective4 encodes a phosphatidylinositol-4-phosphate phosphatase required for proper root hair development in Arabidopsis thaliana. Plant Cell 20: 381-395
Pubmed: Author and Title
Google Scholar: Author Only Title Only Author and Title

Weigel D, Glazebrook J (2006) EMS Mutagenesis of Arabidopsis Seed. CSH Protoc 2006
Pubmed: Author and Title
Google Scholar: Author Only Title Only Author and Title

Xiao Y, Stegmann M, Han Z, DeFalco TA, Parys K, Xu L, Belkhadir Y, Zipfel C, Chai J (2019) Mechanisms of RALF peptide perception by a heterotypic receptor complex. Nature 572: 270-274
Pubmed: Author and Title
Google Scholar: Author Only Title Only Author and Title

Yu F, Li J, Huang Y, Liu L, Li D, Chen L, Luan S (2014) FERONIA receptor kinase controls seed size in Arabidopsis thaliana. Mol Plant 7: 920-922
Pubmed: Author and Title
Google Scholar: Author Only Title Only Author and Title

Yu F, Qian L, Nibau C, Duan Q, Kita D, Levasseur K, Li X, Lu C, Li H, Hou C, Li L, Buchanan BB, Chen L, Cheung AY, Li D, Luan S (2012) FERONIA receptor kinase pathway suppresses abscisic acid signaling in Arabidopsis by activating ABI2 phosphatase. Proc Natl Acad Sci U S A 109: 14693-14698
Pubmed: Author and Title
Google Scholar: Author Only Title Only Author and Title